Cell Reports

Article

Interleukin-10 induces interferon-γ-dependent emergency myelopoiesis

Graphical abstract

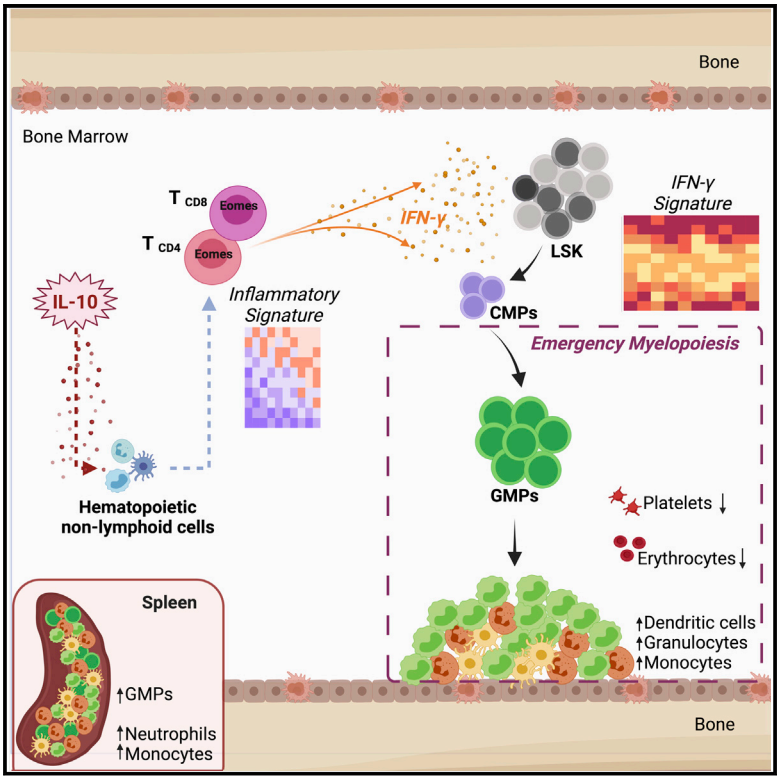

Highlights

- IL-10 expression *in vivo* leads to multiple hematological changes including anemia
- IL-10 expression *in vivo* causes emergency myelopoiesis by inducing IFN-γ production
- CD4 and CD8 T cells exposed to IL-10 express IFN-γ, Eomes, and inflammatory markers

Authors

Ana Cardoso, Ana Catarina Martins, Ana Raquel Maceiras, ..., Yan Li, Paulo Vieira, Margarida Saraiva

Correspondence

ana.cardoso@crick.ac.uk (A.C.), paulo.vieira@pasteur.fr (P.V.), margarida.saraiva@ibmc.up.pt (M.S.)

In brief

Cardoso et al. report that *in vivo* IL-10 exposure causes emergency myelopoiesis, which is accompanied by hematologic alterations in the blood and spleen. IL-10-induced emergency myelopoiesis depends on T cells and IFN-γ. IL-10 reprograms both CD4 and CD8 T cells, inducing expression of IFN-γ, Eomes, and inflammatory and cytotoxic markers.

Cardoso et al., 2021, Cell Reports *37*, 109887
October 26, 2021
https://doi.org/10.1016/j.celrep.2021.109887

CellPress

Cell Reports

CellPress
OPEN ACCESS

Article

Interleukin-10 induces interferon-γ-dependent emergency myelopoiesis

Ana Cardoso,[1,2,3,12,13,*] Ana Catarina Martins,[1,2,4,12] Ana Raquel Maceiras,[1,2] Wei Liu,[5] Isabel Castro,[6,7] António G. Castro,[6,7] António Bandeira,[3,8,9] James P. Di Santo,[8,10] Ana Cumano,[3,8,9] Yan Li,[5,10] Paulo Vieira,[3,8,9,11,*] and Margarida Saraiva[1,2,11,14,*]

[1]i3S-Instituto de Investigação e Inovação em Saúde, Porto, Portugal
[2]IBMC-Instituto de Biologia Molecular e Celular, Universidade do Porto, Porto, Portugal
[3]Department of Immunology, Institut Pasteur, Université de Paris, Unité Lymphocytes et Immunité, 75015 Paris, France
[4]Doctoral Program in Molecular and Cell Biology, Instituto de Cie^ncias Biomedicas Abel Salazar (ICBAS), University of Porto, Porto, Portugal
[5]MOE Key Laboratory of Model Animals for Disease Study, Department of Rheumatology and Immunology, Nanjing Drum Tower Hospital, Chemistry and Biomedicine Innovation Center (ChemBIC), Model Animal Research Center, Nanjing University Medical School, Nanjing University, Nanjing, China
[6]ICVS, University of Minho, Braga, Portugal
[7]ICVS/3B-PT Government Associate Laboratory, Braga/Guimarães, Portugal
[8]INSERM U1223, 75015 Paris, France
[9]University Paris Diderot, Sorbonne Paris Cité, Cellule Pasteur, 75015 Paris, France
[10]Department of Immunology, Institut Pasteur, Université de Paris, Unité Immunité Innée, 75015 Paris, France
[11]Senior authors
[12]These authors contributed equally
[13]Present address: Immunobiology Lab, The Francis Crick Institute, London, UK
[14]Lead contact
*Correspondence: ana.cardoso@crick.ac.uk (A.C.), paulo.vieira@pasteur.fr (P.V.), margarida.saraiva@ibmc.up.pt (M.S.)
https://doi.org/10.1016/j.celrep.2021.109887

SUMMARY

In emergency myelopoiesis (EM), expansion of the myeloid progenitor compartment and increased myeloid cell production are observed and often mediated by the pro-inflammatory cytokine interferon gamma (IFN-γ). Interleukin-10 (IL-10) inhibits IFN-γ secretion, but paradoxically, its therapeutic administration to humans causes hematologic changes similar to those observed in EM. In this work, we use different *in vivo* systems, including a humanized immune system mouse model, to show that IL-10 triggers EM, with a significant expansion of the myeloid progenitor compartment and production of myeloid cells. Hematopoietic progenitors display a prominent IFN-γ transcriptional signature, and we show that IFN-γ mediates IL-10-driven EM. We also find that IL-10, unexpectedly, reprograms CD4 and CD8 T cells toward an activation state that includes IFN-γ production by these T cell subsets *in vivo*. Therefore, in addition to its established anti-inflammatory properties, IL-10 can induce IFN-γ production and EM, opening additional perspectives for the design of IL-10-based immunotherapies.

INTRODUCTION

Emergency myelopoiesis (EM) is a hematopoietic response triggered by stress cues that skew hematopoiesis toward the production of myeloid cells (Boettcher and Manz, 2017). These stress signals often arise after infection, such as by *Plasmodium chabaudi* (Belyaev et al., 2010), *Mycobacterium avium* (Baldridge et al., 2010), Bacillus Calmette-Guérin (BCG) (Kaufmann et al., 2018), or lymphocytic choriomeningitis virus (Schürch et al., 2014). Non-infectious challenges, like irradiation and chemotherapy, can also prompt EM and drive bone marrow (BM) output toward myeloid lineages (Boettcher and Manz, 2017). In many models, the mechanism of EM involves the production of pro-inflammatory cytokines, such as interferon gamma (IFN-γ) (Baldridge et al., 2010; Belyaev et al., 2010; de Bruin et al., 2012; Kaufmann et al., 2018; Schürch et al., 2014). This molecule directs an inflammatory response by hematopoietic stem and progenitor cells, although its effects are context dependent (Baldridge et al., 2010; Belyaev et al., 2010; de Bruin et al., 2012; Kaufmann et al., 2018; Schürch et al., 2014). The role of anti-inflammatory cytokines in modulating hematopoietic responses is less clear.

Interleukin-10 (IL-10) is an anti-inflammatory cytokine that suppresses IFN-γ production through its effects on macrophages and dendritic cells (DCs) (Fiorentino et al., 1989; Moore et al., 1990, 2001; Vieira et al., 1991) thus controlling

immunopathology (Moore et al., 2001). Owing to its strong anti-inflammatory activity, IL-10 was proposed as a promising approach to treat inflammatory diseases (Ouyang and O'Garra, 2019; Saraiva, Vieira and O'Garra, 2020). IL-10 administration in humans, although well tolerated, leads to several hematologic changes also seen in EM, including neutrophilia, monocytosis, anemia, and thrombocytopenia (Huhn et al., 1999; Sosman et al., 2000; Tilg et al., 2002a). However, the mechanisms responsible for these alterations remain unknown, which is a confounding factor for the development of IL-10 as a therapeutic agent (Saraiva et al., 2020).

To elucidate these mechanisms, we used different *in vivo* models, including a previously described mouse model of inducible IL-10 expression, the pMT-10 mouse (Cardoso et al., 2018). We report that increased IL-10 production causes EM, with a significant expansion of the BM myeloid progenitor compartment. This phenotype requires IL-10 receptor signaling, is accompanied by anemia and thrombocytopenia, and is also observed in wild-type (WT) mice expressing IL-10 from a plasmid delivered *in vivo*. Hematopoietic progenitor cells showed a prominent IFN-γ transcriptional signature, and we found that IL-10-driven EM is mediated by IFN-γ. In addition, CD4, CD8, and γδ T cell subsets were found to express elevated levels of IFN-γ and were required for IL-10-driven EM. Notably, delivery of human IL-10 (HpIL-10) to mice with a humanized immune system (HIS mice) also induced expansion of mature and precursor myeloid cells and was accompanied by enhanced production of IFN-γ by T cells.

This work shows that IL-10 skews hematopoiesis toward the myeloid lineage by inducing IFN-γ production in all T cell subsets, unexpectedly revealing that this anti-inflammatory cytokine triggers EM. Our findings explain the hematologic alterations observed in human volunteers receiving therapeutic doses of recombinant IL-10 and are critical to inform the design of IL-10-based therapies.

RESULTS

Induction of IL-10 expression leads to anemia and splenomegaly

To investigate the mechanisms underlying the hematologic changes caused by IL-10 administration, we used a previously characterized transgenic mouse model of IL-10 expression, the pMT-10 mice (Cardoso et al., 2018). IL-10 can be detected in concentrations in the ng/ml range, in the serum of pMT-10 mice as early as 3 days after zinc (Zn) sulfate administration in the drinking water (Cardoso et al., 2018; Figure S1A). This level is comparable to that seen in humans treated with IL-10 (Huhn et al., 1996, 1997, 1999).

We investigated changes in the blood cellularity of pMT-10 mice 30 days after induction of IL-10. Induced mice showed increased numbers of circulating monocytes, decreased numbers of platelets, and reduced hemoglobin levels (Figure 1A). Additionally, an increase in the number of reticulocytes and of the immature platelet fraction (IPF) was observed in the peripheral blood, but no significant changes in the number of white blood cells, lymphocytes, or neutrophils were seen (Figures 1A and S1B). The increase in circulating monocytes, together with thrombocytopenia and anemia, is also observed in humans that receive recombinant IL-10 (Huhn et al., 1996, 1997, 1999). In addition to these hematologic alterations, a pronounced increase in spleen weight and cellularity was observed (Figure 1B). This increase was accompanied by a disruption of splenic architecture and loss of the follicular organization, with no clear separation of the white and red pulp in induced pMT-10 mice (Figure 1C). These alterations were not present in pMT-10 mice deficient for the alpha chain of the IL-10R (pMT-10.IL-10Rα$^{-/-}$) (Figures 1B and 1C), in spite of concentrations of IL-10 in their serum in the order of 40 ng/ml (Figure S1A). Furthermore, they were also absent in control BL/6 receiving normal or Zn-enriched water (Figures S1C and S1D). The IL-10-induced splenomegaly was due to a substantial increase in the number of splenic granulocytes (CD11b$^+$ Gr1$^+$), as B and T cell numbers were unaffected (Figure 1D; see Figure S1E for gating strategy). Again, the expanded splenic myeloid compartment in IL-10-expressing mice was absent in pMT-10.IL-10Rα$^{-/-}$ (Figure 1D) and in control BL/6 mice (Figure S1F). In addition to monocytes (Ly6C^{hi}Ly6G$^-$) and neutrophils (Ly6C$^+$Ly6G$^+$), an increase of DCs (CD11c$^+$) and eosinophils (CD11b$^+$SiglecF$^+$) was observed in the spleen (Figure S1G). No alterations in the cellularity and composition of the thymus were observed 30 days after IL-10 induction (Figures S1H and S1I). The myeloid phenotype readily reversed after interruption of Zn administration (Figure S2).

Collectively, these results showed that IL-10, at doses similar to those therapeutically administered to humans, induced alterations in splenic architecture and prominent myelocytosis, dependent on IL-10 receptor signaling.

IL-10 drives EM

To assess whether the expansion of the peripheral myeloid populations was due to enhanced myelopoiesis, we analyzed the hematopoietic compartments of induced pMT-10 mice. Similar to what we found in the spleen, the BM of IL-10-expressing mice showed a significant increase in the frequency of CD11b$^+$ Gr1$^+$ myeloid cells (Figure 2A; see Figure S3A for gating strategy), particularly of monocytes and DCs (Figure S3B). Immature stages of myeloid differentiation (CD11b$^+$ Gr1$^-$ cells) were also expanded in induced mice (Figure 2A). The frequency of B-lineage cells was significantly reduced, but no alterations were observed in the percentage of BM T cells (Figure 2A).

When we analyzed the progenitor populations in the BM of IL-10 induced mice, the most striking observation was a 50-fold increase in the frequency of lineage$^-$ Sca-1$^+$ c-Kit$^+$ (LSK) cells after induction of IL-10 (Figure 2B). Within the lineage$^-$ Sca-1$^-$ c-Kit$^+$ (LK) population, the number of common myeloid progenitors (CMPs) was decreased, whereas that of granulocyte/macrophage progenitors (GMPs) was increased and that of megakaryocyte/erythrocyte progenitors (MEPs) was not altered (Figures 2B and 2C). The identity of the CMP, GMP, and MEP precursor subpopulations was confirmed by their ability to generate colonies in *in vitro* assays with the same high frequency (virtually 1/1) in both control and induced mice (Table S1). Consistent with the reduction of B-lineage cells in the BM of IL-10-induced mice, we also observed a significant reduction of common lymphoid progenitors (CLPs) (Figure S3C). The number of lymphoid-biased MPP4, on the other hand, was not affected

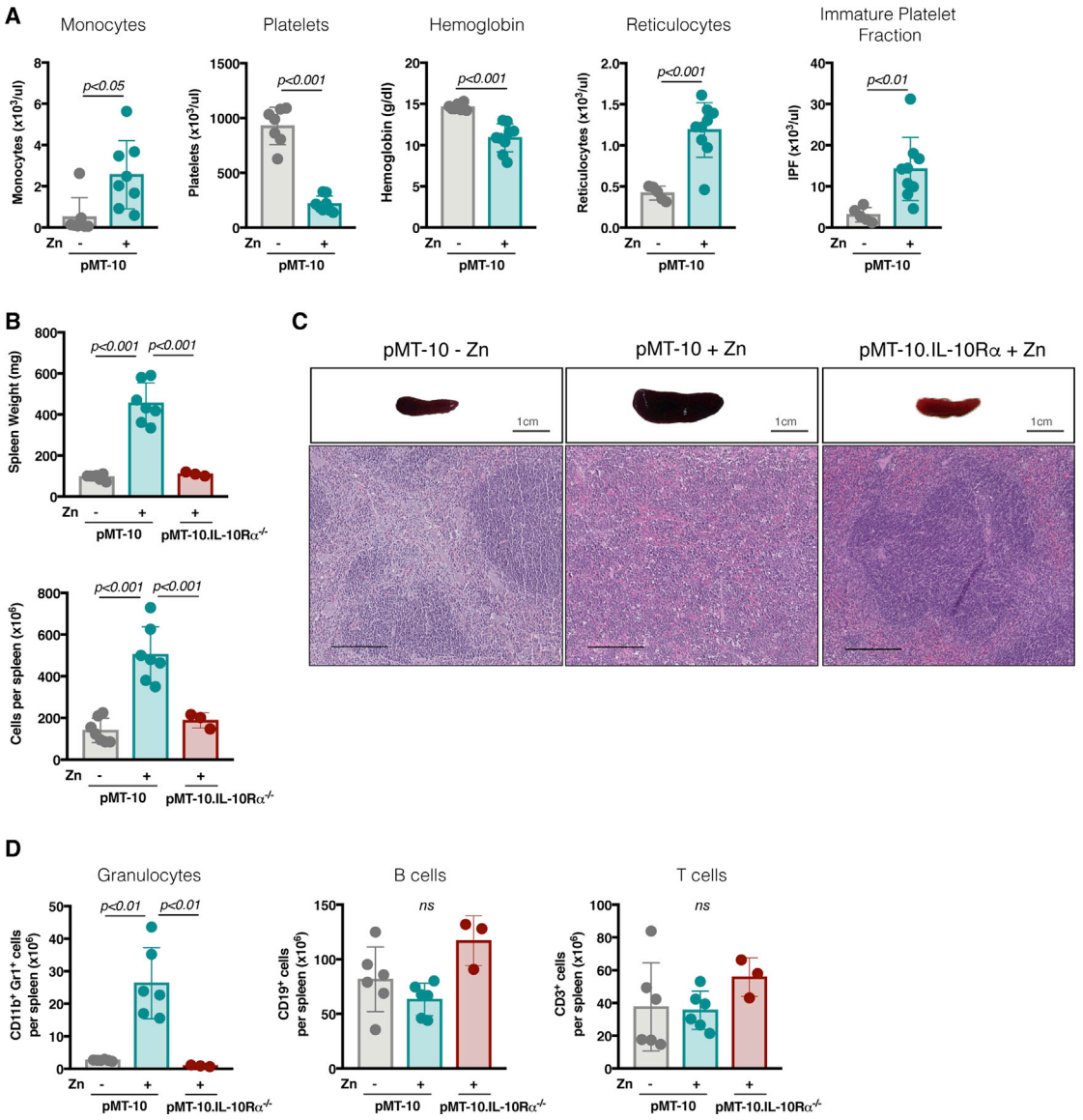

Figure 1. pMT-10 mice overexpressing IL-10 develop anemia, splenomegaly, and increased myeloid cellularity

Normal (–) or Zn-enriched (+) water was fed to mice of the indicated genotypes for 30 days, and their blood and spleen were analyzed.

(A) Number of monocytes, platelets, reticulocytes, immature platelet fraction, and hemoglobin concentration in the blood.

(B) Spleen weight and total cellularity.

(C) Representative images of spleen appearance (top panels; scale bar: 1cm) and histology (H&E) (bottom panels; 100× magnification; scale bar, 200 μm).

(D) Numbers of splenic granulocytes (CD11b$^+$ Gr1$^+$), B cells (CD19$^+$), and T cells (CD3$^+$). Each bar represents the mean ± SD for 3–7 mice, in one of at least two independent experiments. Each dot represents a single mouse. Data were analyzed with Student's t test (A) or one-way ANOVA (B and D). ns, not significant.

(Figure S3D). Furthermore, within the LSK population, no changes were observed in the number of CD150$^+$ CD48$^-$ long-term hematopoietic stem cells (LT-HSCs) (Boyer et al., 2011; Oguro et al., 2013; Figure 2D; Figures S3E and S3F), whereas the total number of the CD150$^+$ CD48$^+$ (MPP2) and CD150$^-$ CD48$^+$ (MPP3) subsets was increased in induced mice (Figure 2D; Figure S3E).

Inflammatory signals may induce upregulation of Sca-1 expression on myeloid precursor populations, possibly leading to the under-estimation of the degree of GMP expansion, as some LK cells with upregulated Sca-1 would be included in the LSK gate (Pietras et al., 2014, 2015). We therefore analyzed the LSK compartment for the expression of endothelial-cell-selective adhesion molecule (ESAM), which identifies LT-HSCs (Sudo et al., 2012). Although the percentage of ESAM$^-$ cells increased in all subpopulations of induced mice, suggesting that some LK cells were included in the LSK gate, most (80%–85%) CD150$^+$CD48$^-$LSKs were ESAM$^+$ (Figure S3E).

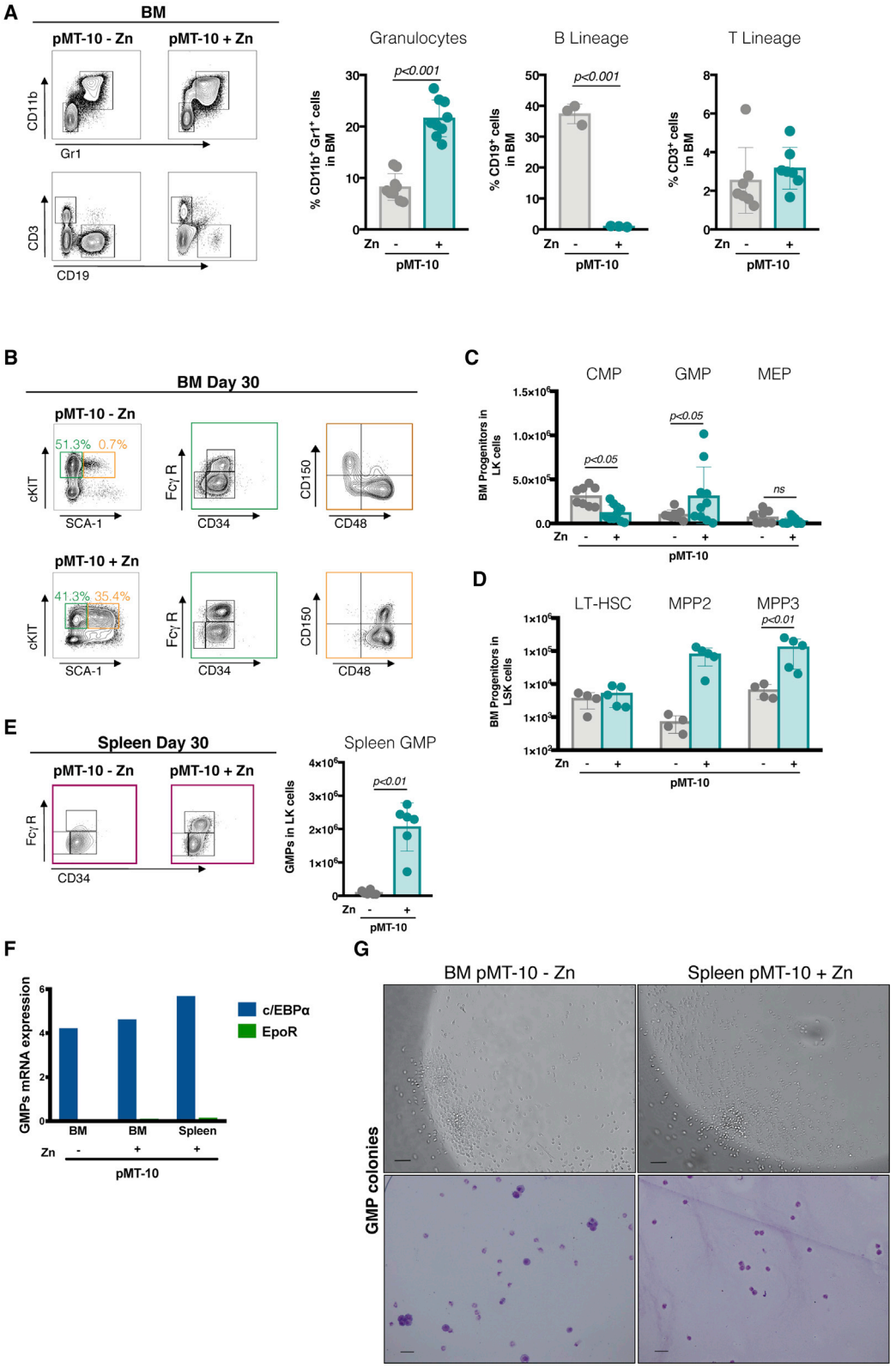

(legend on next page)

Consequently, the number of bona fide LT-HSCs was the same before or after induction (Figure S3F).

Extramedullary myelopoiesis in IL-10-induced mice

We next examined the spleen of induced or control pMT-10 mice for signs of extramedullary myelopoiesis. A prominent population of splenic GMPs was observed in induced pMT-10 mice (Figure 2E), which expressed high levels of *cEBPa* and low levels of *EpoR*, similarly to BM GMPs (Figure 2F). The identity of this GMP population was further attested by their ability to differentiate into mature myeloid cells when cultured *in vitro* (Figure 2G; Table S1). We therefore concluded that EM caused by IL-10 is accompanied by splenic myelopoiesis.

Kinetic analysis of IL-10-induced EM revealed that the expansion of BM LSKs and GMPs is noticeable as early as day 7 after Zn administration (Figure S3G). This result was also true for splenic LSKs, but the expansion of splenic GMPs in induced pMT-10 mice was only significant by day 15 of induction (Figure S3G). Increased mature myeloid cells in the BM (Figure S3H) and circulating granulocytes (Figures S3I and S3J) were evident as early as day 15 post-IL-10 induction.

Hydrodynamic administration of an IL-10-encoding plasmid (pIL-10) causes EM in WT mice

Because the effect of IL-10 on myelopoiesis can be detected early after IL-10 induction, we investigated whether EM could also be observed in a non-transgenic system, in which a transient high concentration of IL-10 is achieved by hydrodynamic delivery of an pIL-10 to BL/6 mice (Li et al., 2017). In this system, a plasmid directing expression of a cytokine is administered intravenously in a large volume of PBS, leading to short-lived production of high levels of the cytokine (Li et al., 2017). The serum concentration of the cytokine typically peaks on day 1 and then rapidly decays to subnanomolar concentrations by day 7 (Li et al., 2017; Ortaldo et al., 2005; Sato et al., 2006).

On day 4 post-delivery, BL/6 mice injected with pIL-10 had high levels of IL-10 in their sera (10–40 ng/ml; Figure 3A) and showed an increase in the BM GMP population, as compared to mice injected with PBS or with an empty plasmid (Figure 3B). Administration of the plasmid to pMT-10.IL-10R$\alpha^{-/-}$ did not increase the BM GMP frequency (Figure 3C) in spite of the high levels of IL-10 in their sera (Figure 3A), demonstrating that the effect is IL-10 receptor signaling specific. By 7 days post-administration, mice overexpressing IL-10 displayed marked splenomegaly with increased cellularity (Figure 3D) and a prominent population of GMPs in this organ (Figure 3E).

As expected, no IL-10 was detected in the absence of the plasmid or in mice that received a control empty plasmid (Figure 3A), and also no expansion of GMP was observed in either group (Figures 3B and 3C). This result confirms that PBS and empty plasmid can be used as experimental controls for the hydrodynamic delivery of a cytokine-encoding plasmids, as previously reported (Li et al., 2017).

We concluded that the rapid induction of IL-10 (to levels above 10 ng/ml in the serum) causes EM also in WT mice, consistent with our observations in the pMT-10 transgenic system.

Induction of EM by IL-10

All progenitor populations, namely, LSKs, CMPs, and GMPs, expressed similar levels of both chains of the IL-10R in control and induced mice (Figure S4A). To investigate whether IL-10 induced EM by directly signaling on hematopoietic progenitors, we reconstituted pMT-10.IL-10R$\alpha^{-/-}$ recipients with a 1:1 ratio of IL-10R$\alpha^{+/+}$ (BL/6 Ly 5.1) and IL-10R$\alpha^{-/-}$ (Ly 5.2) BM precursors. Induction of IL-10 expression in these mixed chimeras caused EM, as attested by the expansion of BM GMPs and LSKs (Figure 4A), but the 1:1 ratio between the IL-10R$\alpha^{+/+}$ and the IL-10R$\alpha^{-/-}$ genotypes was maintained (Figure 4B). Thus, IL-10 signaling on hematopoietic progenitors is not strictly required for the expansion of GMPs and EM development. Consequently, although direct signaling by IL-10 may play a role in EM, other factors, produced in response to IL-10 induction, are likely to be involved in mediating the myelopoietic phenotype observed.

IL-10 driven myeloexpansion requires IFN-γ expression

Because the expanded population of CD34^{+}FcγR^{+} LSKs represents bona fide GMPs (Figures 2F and 2G; Table S1), we hypothesized that IL-10 induction led to enhanced differentiation of GMPs from earlier progenitors. We therefore reasoned that an analysis of the populations upstream of GMPs would provide important information about the mechanism underlying IL-10-induced EM. Thus, we compared the transcriptome of progenitor populations from pMT-10 or BL/6 control mice fed with Zn (Figure S4B).

Global transcriptome analysis of CMPs showed that 308 genes were differentially expressed in induced pMT-10 mice as compared to BL/6 (179 genes upregulated [logFC > 2 and p value < 0.05] and 129 genes downregulated [logFC < 2 and p value < 0.05]) (Figure 4C). Gene set enrichment analysis

Figure 2. IL-10 drives BM and extramedullary myeloexpansion

Normal (–) or Zn-enriched (+) water was fed to pMT-10 mice for 30 days.

(A–E) On day 30, BM (A–D) and (E) spleen cell suspensions were stained for mature or hematopoietic progenitor subsets. (A) Representative plots and frequencies of BM granulocytes, B lineage, and T cells. (B) Representative plots and frequency of BM LK (Lin^{-} IL-7Rα^{-}cKit^{+}Sca-1^{-}) and LSK (Lin^{-} IL-7Rα^{-}cKit^{+}Sca-1^{+}) compartments. Numbers of CMP (Lin^{-}IL-7Rα^{-}c-Kit^{+}Sca-1^{-}FcγR^{lo}CD34^{+}), GMP (Lin^{-}IL-7Rα^{-}c-Kit^{+}Sca-1^{-}FcγR^{+}CD34^{hi}), and MEP (Lin^{-}IL-7Rα^{-}c-Kit^{+}Sca-1^{-}FcγR^{-}CD34^{lo}) populations (C) and LSK cells: LT-HSC (Lin^{-}IL-7Rα^{-}c-Kit^{+}Sca-1^{+}CD150^{+}CD48^{-}), MPP2 (Lin^{-}IL-7Rα^{-}c-Kit^{+}Sca-1^{+}CD150^{+}CD48^{+}), and MPP3 (Lin^{-}IL-7Rα^{-}c-Kit^{+}Sca-1^{+}CD150^{-}CD48^{+}) (C).

(E) Representative FACS plots and numbers of splenic GMP at day 30 of IL-10 induction.

(F) Transcriptional analysis of FACS-sorted GMPs for the expression of c/EBPα and EpoR, normalized for the expression of HPRT.

(G) Top panels: representative images of colonies obtained from BM or splenic GMPs sorted from the BM and differentiated for 6 days in culture (100×; scale bar, 100 μm); bottom panels: May-Grünwald staining of the cells in the culture (200×; scale bar, 100 μm). Each bar (A–E) represents the mean ± SD for 4–10 mice, from at least 2 independent experiments. Each dot represents a single mouse. Data were analyzed with Student's t test. In (F), each bar represents samples from 3–6 mice pooled, and the scale represents arbitrary units.

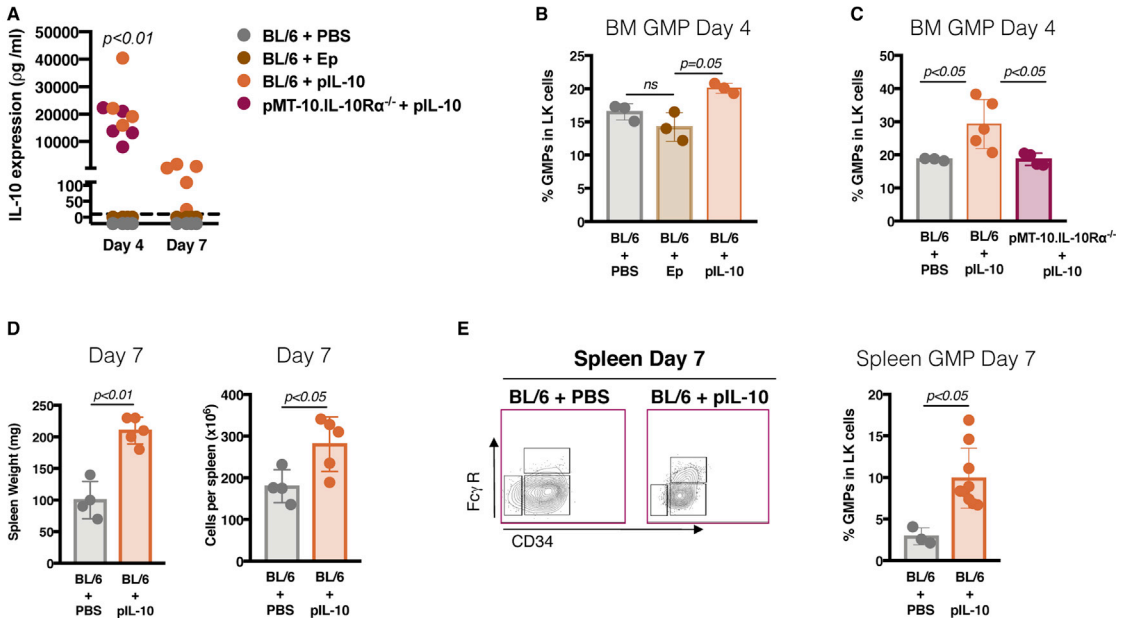

Figure 3. The IL-10-driven myelopoiesis is phenocopied by hydrodynamic delivery of an IL-10-encoding plasmid

An IL-10-expressing plasmid (pIL-10) was injected into BL/6 or pMT-10.IL-10Rα$^{-/-}$ mice, diluted in PBS. As a control, vehicle (PBS) alone or an empty plasmid (Ep) was used.

(A) Four and 7 days post-injection, IL-10 levels were assessed in the serum.

(B and C) B progenitor subsets were analyzed as before, at day 4 post injection.

(D) Spleen weight and total number of leukocytes were assessed at day 7.

(E) Representative plots and frequencies of splenic GMPs at day 7 post pIL-10 administration. Each bar represents the mean ± SD, for 3–8 mice from 2 experiments. Each dot represents a single mouse. Data were analyzed with one-way ANOVA (B and C) and Student's t test (D and E). ns, not significant.

(GSEA) of these genes was performed with mouse hallmark gene sets (Liberzon et al., 2015; Subramanian et al., 2005). Of the 50 gene sets tested, 9 were found to be significantly upregulated in CMPs from pMT-10 mice versus CMPs from BL/6 mice (Figure 4D). The highest scoring gene set, with a normalized enrichment score (NES) of 2.70, was the IFN-γ response pathway (Figure 4D), and an analysis of the top 30 of the 308 differentially expressed genes revealed an IFN-γ-dominated transcriptional signature (Figure 4E). Indeed, 22 of these 30 genes were part of the list of IFN-γ regulated genes (IRGs) from the Interferome database (Rusinova et al., 2013), of which 8 were also included in an IFN-γ-dominated disease module recently published (Singhania et al., 2019) (Figure 4E). This signature was also evident when all 308 altered genes are considered because 110 of them were IRGs (Figure S4C). This IFN-γ-dominated transcriptional signature was already detectable in LT-HSC and MPP2 subsets from induced pMT-10 mice (Figure S4D). Of note, CMPs and GMPs expressed both chains of the IFN-γR (Figure S4E).

Given the pronounced IFN-γ signature described above, the role of IFN-γ in some models of EM (Baldridge et al., 2010; Belyaev et al., 2010; de Bruin et al., 2012; Kaufmann et al., 2018; Schürch et al., 2014), and previous observations that suggested that IL-10 can induce expression of IFN-γ in *in vivo* models (Emmerich et al., 2012a, 2012b; Mumm et al., 2011; Naing et al., 2016, 2018; Tilg et al., 2002a), we considered IFN-γ as the strongest candidate to mediate the IL-10-induced EM. Other candidates included IFN-α, whose pathway overlaps extensively with that of IFN-γ (153 of 187 genes are common to both pathways) but can inhibit myelopoiesis (Khan et al., 2020; Smith et al., 2018), and other inflammatory cytokines such as IL-6 and TNF-α, which had a much lower NES. Thus, we first investigated the contribution of IFN-γ to IL-10-driven myeloexpansion. As shown in Figures 4F–4H, pMT-10.IFN-γ$^{-/-}$ mice did not develop splenomegaly (Figure 4F), expansion of splenic granulocytes (Figure 4G), or expansion of GMP in the BM (Figure 4H) 30 days after induction of IL-10 expression.

Collectively, the above findings indicate that IFN-γ mediates IL-10-induced myeloexpansion, although they do not exclude that other inflammatory mediators, which on their own could not sustain EM, may also contribute to IL-10 induced myeloexpansion.

Despite the clear IFN-γ dominated transcriptomic signature and its key role in EM, the serum levels of this cytokine in induced mice were below detection throughout the duration of the experiment (Figure S4F), suggesting a localized action in the BM. We also did not detect IFN-α, IL-1β, transforming growth factor α (TNF-α), macrophage colony-stimulating factor (M-CSF), or granulocyte-macrophage colony-stimulating factor (GM-CSF), but low levels of G-CSF were found in both induced and control animals (Figure S4F). Low levels of IL-6 were also detected in induced mice, possibly because of the increased number of monocytes/macrophages that resulted from EM (Figure S4F).

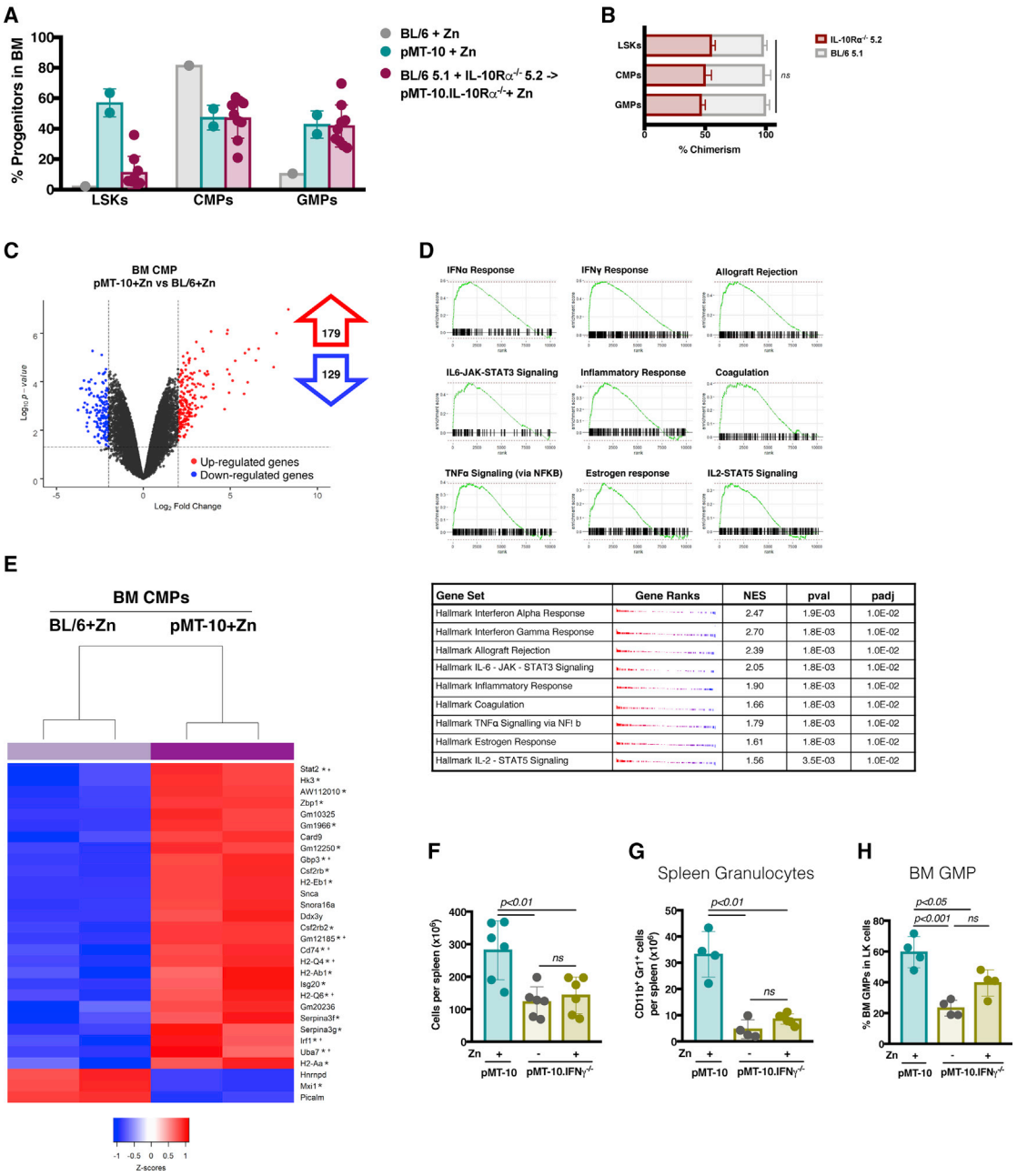

Gene Set	Gene Ranks	NES	pval	padj
Hallmark Interferon Alpha Response		2.47	1.9E-03	1.0E-02
Hallmark Interferon Gamma Response		2.70	1.8E-03	1.0E-02
Hallmark Allograft Rejection		2.39	1.8E-03	1.0E-02
Hallmark IL-6 - JAK - STAT3 Signaling		2.05	1.8E-03	1.0E-02
Hallmark Inflammatory Response		1.90	1.8E-03	1.0E-02
Hallmark Coagulation		1.66	1.8E-03	1.0E-02
Hallmark TNFα Signalling via NFI b		1.79	1.8E-03	1.0E-02
Hallmark Estrogen Response		1.61	1.8E-03	1.0E-02
Hallmark IL-2 - STAT5 Signaling		1.56	3.5E-03	1.0E-02

Figure 4. CMPs isolated from mice overexpressing IL-10 show an IFN-γ transcriptional signature and IFN-γ is required for myeloexpansion

pMT-10.IL-10Rα$^{-/-}$ recipients were reconstituted with a 1:1 ratio of control (Ly5.1) and IL-10Rα$^{-/-}$ (Ly5.2) precursors (4 × 10^6 total T-depleted BM donor cells). Five weeks after reconstitution, Zn-enriched water was administered to the animals for 2 weeks.

(A) Percentage of LSKs, CMP, and GMPs in the BM of the reconstituted mice.

(B) Chimerism within the LSK, CMP, and GMP compartments.

(C) Volcano plot depicting the gene expression differences of pMT-10 CMPs when compared to BL/6 CMPs.

(D) The nine mouse hallmark gene sets significantly (padj < 0.05) enriched in CMPs from pMT-10+Zn mice versus CMPs from BL/6+Zn mice, as determined by GSEA. Individual enrichment plots of the nine significant gene sets from the GSEA analysis are shown in the table below. NES, normalized enrichment score; pval, enrichment p value; padj, Benjamini-Hochberg-adjusted p value.

(E) Heatmap of the top 30 differentially expressed genes in BM CMPs of pMT-10 or BL/6 mice induced with Zn. Genes associated with IFN γ signaling are marked with either * (Interferome database) or † (an IFN-γ related module; see Singhania et al., 2019). *Z* scores are color coded as shown in the scale at the bottom.

(F–H) Total number of splenocytes (F), number of splenic granulocytes (G), and frequency of BM GMPs (H) determined for the indicated groups, before (–) or after (+) 30 days of induction. Bars represent the mean ± SD for 3–6 mice, from 2 independent experiments. Each dot represents a single mouse. Data were analyzed with one-way ANOVA. ns, not significant.

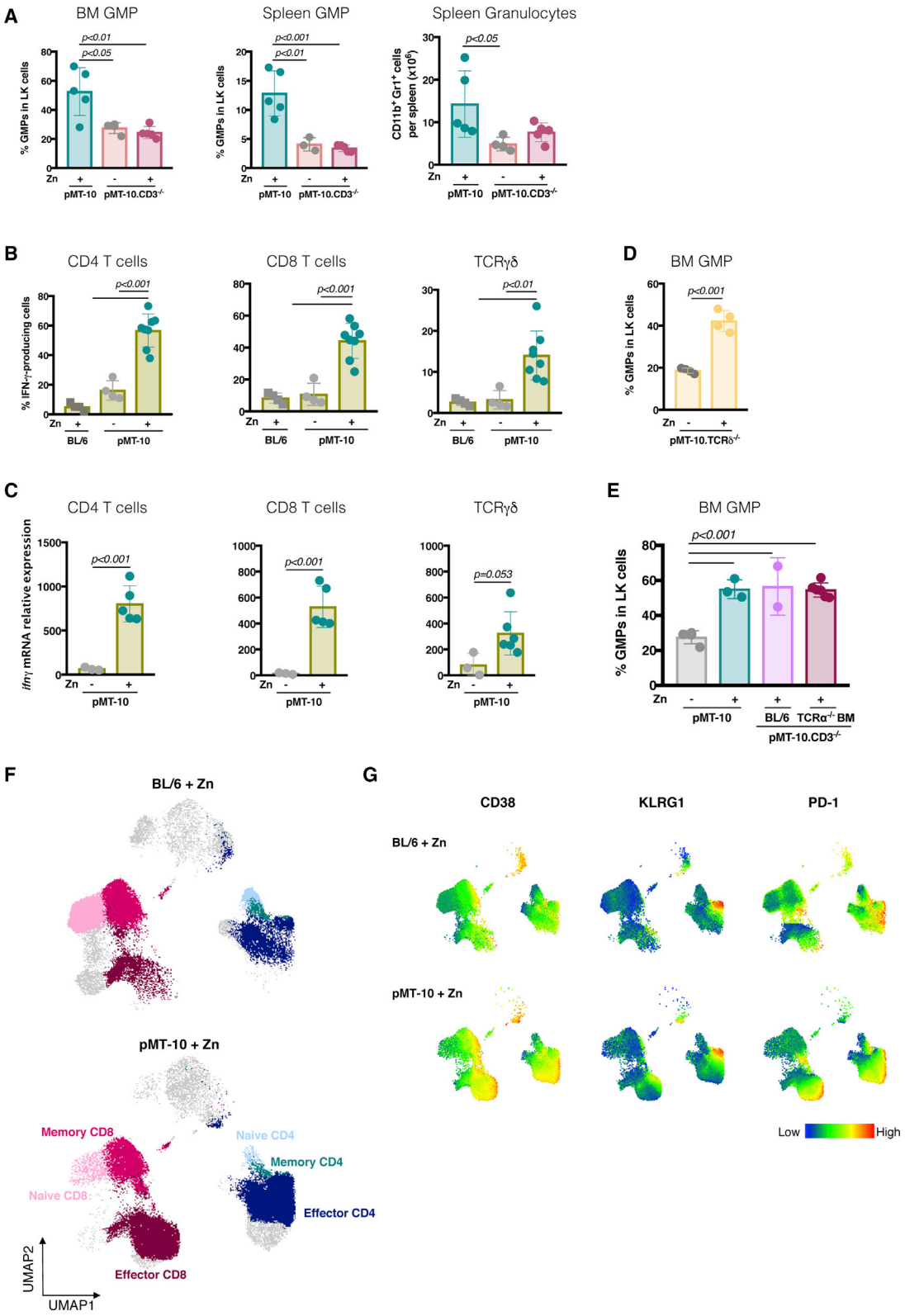

(legend on next page)

T cells are key players in IL-10-driven EM

To search for the cellular source of IFN-γ, we induced IL-10 expression in pMT-10.Rag.γc$^{-/-}$ mice. These mice showed no signs of EM and had normal representation of splenic GMPs and mature granulocytes (Figure S5A), indicating that a lymphoid population is required for IL-10-mediated EM. Induced pMT-10.Rag$^{-/-}$ mice also failed to show an expansion of splenic GMPs or granulocytes (Figure S5B), indicating that natural killer (NK) cells and innate lymphoid cells (ILCs) alone are not able to drive the phenotype. In contrast, pMT-10.μMT$^{-/-}$ showed an expansion of BM GMPs (Figure S5C), demonstrating that B cells are not necessary. We then investigated the contribution of T cells. Induced pMT-10.CD3$^{-/-}$ mice did not develop EM and did not show an expansion of BM or splenic GMPs or of peripheral granulocytes (Figure 5A).

Because T cells and IFN-γ were both required for IL-10-induced EM and because T cells are major producers of IFN-γ, we analyzed which T cell subsets expressed IFN-γ *in vivo*, after IL-10 induction. A substantial increase in the frequency of BM CD4, CD8, and γδ T cells producing IFN-γ upon *in vitro* restimulation with PMA/ionomycin was observed in induced pMT-10 mice (Figure 5B). In addition, all *ex vivo* purified CD4, CD8, and γδ BM T cell populations showed more than 100-fold upregulated transcription of the *Ifng* gene (Figure 5C). Of note, the frequency of non-T cells (which include NK cells and ILCs) secreting IFN-γ in the BM, although slightly increased in induced mice, is very low, and over 95% of IFN-γ^{+} cells are also CD3^{+} (Figure S5D). Taken together, these results highlighted T cells as the major cellular source of IFN-γ during IL-10-induced EM.

To determine if a particular T cell population played a more important role, we induced IL-10 expression in pMT-10.TCRδ$^{-/-}$ mice (which only have αβ T cells) and in pMT-10.CD3$^{-/-}$ mice reconstituted with TCRα$^{-/-}$ BM progenitors (which only have γδ T cells). Both groups of mice showed the characteristic expansion of BM GMPs seen in IL-10-expressing pMT-10 mice (Figures 5D and 5E). Therefore, we concluded that both αβ and γδ T cells can be the source of the IFN-γ required for IL-10-induced EM.

We studied the phenotype of BM CD4 and CD8 T cells during IL-10 induction with a detailed analysis of the expression of surface markers. The analysis was restricted to CD4 and CD8 T cells, in view of the paucity of Tγδ cells in the BM. Dimensionality reduction analysis (Becht et al., 2018) showed that the effector compartments of CD4 and CD8 T cells were expanded in the BM of induced pMT-10 mice undergoing EM, whereas the percentage of naive T cells was reduced (Figure 5F; Figure S6A). A more detailed analysis showed an increased expression of CD38 and PD-1 in both CD4 and CD8 T cells (Figure 5G), indicating a high level of activation.

Mechanism of IFN-γ induction in T cells

To investigate in more detail the functional changes in the T cell compartment during IL-10 induction, we performed targeted RNA sequencing (RNA-seq) in fluorescence-activated cell sorting (FACS)-purified BM T cells from induced pMT-10 mice. Upon IL-10 induction, 267 and 187 genes were significantly upregulated (logFC > 2 and $p < 0.05$) and 301 and 15 were significantly downregulated (logFC < 2 and $p < 0.05$), in CD4 and CD8 T cells, respectively (Figure 6A). Thus, IL-10 exposure *in vivo* led to a transcriptional reprograming that is more pronounced for CD4 T cells than for CD8 T cells. Such reprograming was not observed in the absence of Zn or in BL/6 mice fed with Zn (Figure 6B). Among the top 50 differentially expressed genes in CD4 and CD8 T cells, we found, as expected, IFN-γ, but also genes encoding several inflammatory chemokines, such as CCL3 (MIP1α), CCL4 (MIP1β), and CCL5 (RANTES); cytotoxic molecules, as Perforin 1, Granzyme B, and Granzyme K; and activation markers, as CD38 and Ly6a (Figure 6B). Several of these genes are known to be upregulated by IFN-γ (annotated with * in Figure 6B), suggesting that the BM CD4 and CD8 T cells not only secreted this cytokine but also responded to it. In line with this finding, we detected the expression of the *IfngR1* and *IfngR2* genes in both CD4 and CD8 T cells, although upon IL-10 induction, CD4 T cells downregulated the expression of these genes (Figure S6B), as described (Bach et al., 1995).

Among the top 50 genes upregulated in BM CD4 T cells was Eomesodermin (*Eomes*) (Figure 6B), a transcription factor mainly associated with IFN-γ expression in CD8 T cells (Istaces et al., 2019; Pearce et al., 2003; Yang et al., 2008). In contrast, *Tbx21* (Tbet), a transcription factor known to control IFN-γ expression in CD4 T cells (Cano-Gamez et al., 2020; Kaech and Cui, 2012; Szabo et al., 2000; Yang et al., 2008), was not differentially expressed, neither in CD4 nor in CD8 T cells. This result was confirmed by qPCR in FACS-purified BM CD4 and CD8 T cells (Figure S6C). Furthermore, combined intracellular staining showed that IFN-γ-producing CD4 and CD8 T cells were Eomes^{+} (Figure 6C), but none of these subsets showed significant staining for Tbet (Figure 6D). These observations suggest that IFN-γ expression by CD4 and CD8 T cells in response to IL-10 *in vivo* is regulated by Eomes.

Collectively, our findings support the conclusion that the transcriptional and functional reprograming of CD4 and CD8 T cells that occurred after IL-10 induction are comparable to those seen

Figure 5. T cells are required for IL-10-driven myeloexpansion

(A) Frequencies of BM and spleen GMP and number of splenic granulocytes of non-induced (–) or induced (+) pMT-10 and pMT-10.CD3$^{-/-}$ after 15 days of Zn.

(B) Percentages of IFN-γ-producing CD4, CD8, or TCRγδ cells in the BM of the indicated mice.

(C) Expression of the *Ifng* gene in sorted BM CD4, CD8, or TCRγδ T cell subsets from non-induced (–) or induced (+) pMT-10 mice. The level of expression was normalized to that of HPRT, and the result is presented as arbitrary units.

(D) Percentage of GMP in the BM of pMT-10.TCRδ$^{-/-}$ before (–) or after (+) 30 days of induction of IL-10.

(E) Frequency of GMP in the BM of the indicated chimeric mice, after 5 weeks of reconstitution and 2 weeks of induction.

(F) Uniform manifold approximation and projection (UMAP) analysis of flow cytometry data overlaying different immune populations, namely, effector (CD44^{+} CD62L^{-}), memory (CD44^{+} CD62L^{+}), or naive (CD44^{-} CD62L^{+}) CD4 or CD8 T cells, as identified with manual gating (Figure S6A).

(G) CD38, PD-1, and KLRG1 intensity in BM T cells from control versus induced pMT-10 mice. In (A)–(E), each bar represents the mean ± SD for 3–8 independent mice, from one (D and E) or two (A–C) independent experiments, and each dot represents a single mouse. Data were analyzed with one-way ANOVA (A, B, and E) or Student's t test (C and D).

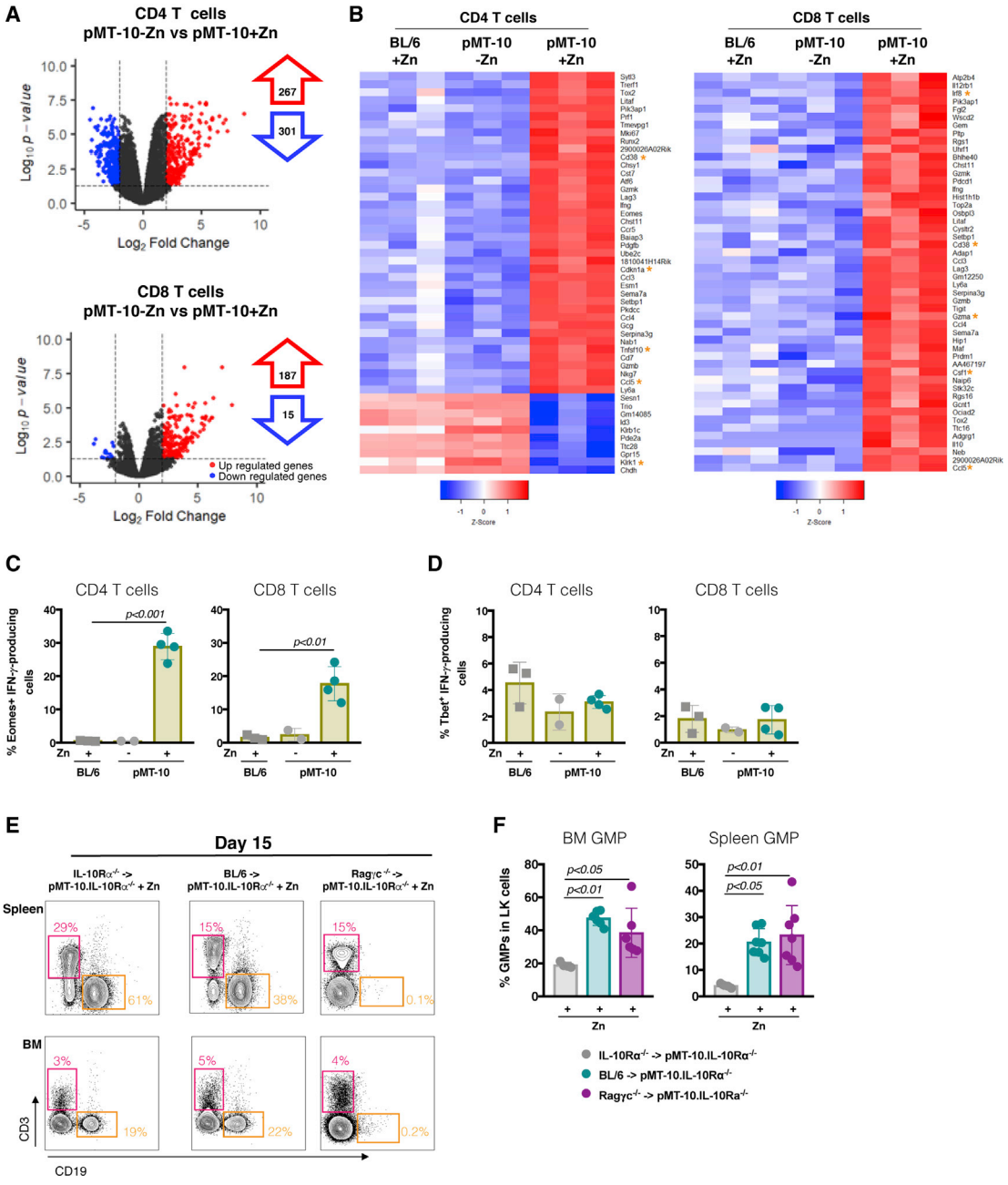

Figure 6. *In vivo* IL-10 exposure reprograms CD4 and CD8 T cells

(A) Volcano plots depicting gene expression differences between BM CD4 and CD8 T cells from pMT-10 fed with normal or Zn-enriched water.

(B) Heatmap showing the top 50 differentially expressed genes in BM CD4 and CD8 T cells, when comparing induced (pMT-10+Zn) with control (BL/6+Zn and pMT-10-Zn) mice.

(C) Eomes-positive IFN-γ-producing CD4 and CD8 cells.

(D) Tbet-positive IFN-γ-producing CD4 and CD8 cells.

(E) Representative FACS plots and frequencies of $CD3^+$ and $CD19^+$ cells in the spleen and BM of the indicated chimeric mice after 5 weeks of reconstitution and 2 weeks of induction.

(F) Percentage of GMPs in the BM and spleen of the reconstituted mice shown in (E) Bars represent the mean ± SD, for 2–7 mice from 1 experiment (C and D) or 2 experiments (E and F). Each dot represents a single mouse. Data were analyzed with Student's t test (C and D) or one-way ANOVA (F).

under strong inflammatory conditions (Kaech and Cui, 2012; Takeuchi and Saito, 2017).

Both CD4 and CD8 T cells expressed Il10rα and β (Figure S6D); therefore, we studied whether the CD4 and CD8 reprograming observed upon IL-10 induction would be caused by a direct action of IL-10 in T cells, as previously observed in a tumor model (Emmerich et al., 2012b). By reconstituting lethally irradiated pMT-10.IL-10Rα$^{-/-}$ mice with Rag γc$^{-/-}$ BM, virtually all hematopoietic cells in the chimeras derive from the donor HSC inoculum (i.e., they are Rag γc$^{-/-}$), with the exception of a population of recipient-derived T cells that survive the irradiation and expand (Komatsu and Hori, 2007; Mercier et al., 2016). As shown in Figure 6E, these chimeric mice retained a prominent population of splenic and BM T cells, of circa 15% and 4% respectively, which are IL-10Rα deficient, because they are recipient derived. In contrast, CD19^{+} cells are virtually absent from both spleen and BM of the reconstituted mice because they cannot be generated from Rag γc$^{-/-}$ precursors (Figure 6E). Induction of IL-10 in these mice caused EM, as shown by the expansion of both BM and splenic GMPs, similarly to what is observed in pMT-10.IL-10Rα$^{-/-}$ reconstituted with WT BL/6 precursors (Figure 6F). As expected, (see above Figures 1B–1D), when IL-10Rα$^{-/-}$ HSCs are used to reconstitute pMT-10.IL-10Rα$^{-/-}$ mice, no expansion of GMPs is observed (Figure 6F).

Therefore, we concluded that direct IL-10 signaling on T cells is not necessary to induce IFN-γ production, although direct mechanisms may also operate, as has been suggested (Emmerich et al., 2012a; Mumm et al., 2011; Naing et al., 2016, 2018).

IL-10 induces myeloexpansion and IFN-γ-producing T cells in mice with a humanized immune system

Given that our findings provide an explanation for some of the secondary effects associated with the administration of therapeutic doses of IL-10 to humans (Huhn et al., 1996, 1997, 1999), we next sought to investigate the effect of IL-10 elevation on the human immune system by using HIS mice (Li et al., 2017; Figure S7) hydrodynamically injected with a plasmid encoding HpIL-10. Similar to what was seen in the mouse model (Figure 3), HIS mice administered with HpIL-10 showed splenomegaly (Figure 7A), with the expansion of myeloid cells (Figure 7B) and of GMPs in the spleen (Figure 7C). The paucity of BM T cells in HIS mice precluded the analysis of IFN-γ in this compartment; however, a higher frequency of both CD4 and CD8 IFN-γ-producing T cells in the spleen was observed (Figure 7D). Taken together, these results establish that both in murine and human hematopoiesis, elevated IL-10 production, to levels comparable to those obtained during therapeutic administration, induce EM dependence on IFN-γ, which is mostly produced by T cells.

DISCUSSION

IL-10, a potent anti-inflammatory cytokine expressed by most immune cells, inhibits macrophage and DC function and limits the production of IFN-γ by T helper 1 (Th1) effector cells *in vitro* (Moore et al., 2001; Ouyang and O'Garra, 2019; Saraiva et al., 2020). Nevertheless, CD4^{+} T cells differentiated under conditions of strong T cell receptor (TCR) stimulation in the presence of IL-12 produce both IFN-γ and IL-10, thus ensuring a negative feedback loop to avoid excessive inflammation and limit immunopathology (O'Garra and Vieira, 2007; Saraiva et al., 2009). Consistent with this view, disruption of the IL-10/IL-10R axis in both mice and humans is associated with exacerbated inflammation (Moore et al., 2001). Therefore, the therapeutic use of IL-10 has been tested in the context of several inflammatory disorders, although with limited success so far (Huhn et al., 1996, 1997, 1999; Naing et al., 2016; Tilg et al., 2002b).

In this work, we reveal an unexpected effect of IL-10 *in vivo* as a trigger of EM. We use two different models, which mimic the depot effects of therapeutically administered pegylated IL-10 and avoid the stress resulting from repeated injections. We show that elevated levels of IL-10 drive the expansion of LSKs and GMPs in the BM and spleen and promote the differentiation of myeloid cells at the expense of other lineages. In consequence, IL-10-induced animals accumulate monocytes and granulocytes in the periphery and have a reduced number of platelets and hemoglobin concentration in the blood. Moreover, an increased number of reticulocytes and reticulated platelets is observed in the peripheral blood of induced pMT-10 mice. This result could suggest an increased sequestration of platelets and red blood cells in the spleen or clearance at the periphery. The overall phenotype, which reflects the alterations reported in humans receiving therapeutic doses of this cytokine (Emmerich et al., 2012b; Huhn et al., 1996, 1997, 1999; Mumm et al., 2011), is also observed upon hydrodynamic delivery of IL-10 to WT mice or to mice carrying a humanized hematopoietic system (HIS mice). Of note, the enhanced myelopoiesis is rapidly reversed once IL-10 levels return to normal, as is also the case of the hematologic alterations detected in humans receiving IL-10 (Huhn et al., 1996, 1997, 1999).

Other mouse models expressing IL-10 constitutively, under the control of the major histocompatibility complex class II (MHC class II) promoter (Groux et al., 1999) or the macrophage-specific CD68 promoter (Lang et al., 2002), have been described, but no alterations in myeloid populations were reported. However, the concentration of IL-10 in the serum of these mice was only in the subnanomolar range (Groux et al., 1999; Lang et al., 2002), suggesting that either constitutive low levels of IL-10 are insufficient to enhance myeloid cell production or only rapid increases in circulating IL-10 trigger EM. It is important to note, at any rate, the specificity of our systems because EM required IL-10 signaling and was absent in IL-10Rα-deficient animals.

We show that IL-10-driven EM was dependent on T cells and on IFN-γ, of which most was produced by T lymphocytes in the BM. IFN-γ-induced EM is consistent with the known effect of this cytokine in other infection models (Belyaev et al., 2010, 2013; de Bruin et al., 2012; Kaufmann et al., 2018). However, the finding that IL-10 led to T cell production of IFN-γ is surprising, in view of the ability of IL-10 to inhibit IFN-γ secretion by T cells *in vitro*, which was the basis for the cloning of this cytokine (Fiorentino et al., 1989; Moore et al., 1990; Vieira et al., 1991), and the multiple reports that abrogation of IL-10 signaling during infection results in increased IFN-γ (Moore et al., 2001). Such a paradoxical effect of IL-10 *in vivo* has been noted in Crohn's disease patients (Tilg et al., 2002b) and in murine tumor models (Naing et al., 2018), in which IL-10 was found to induce elevated

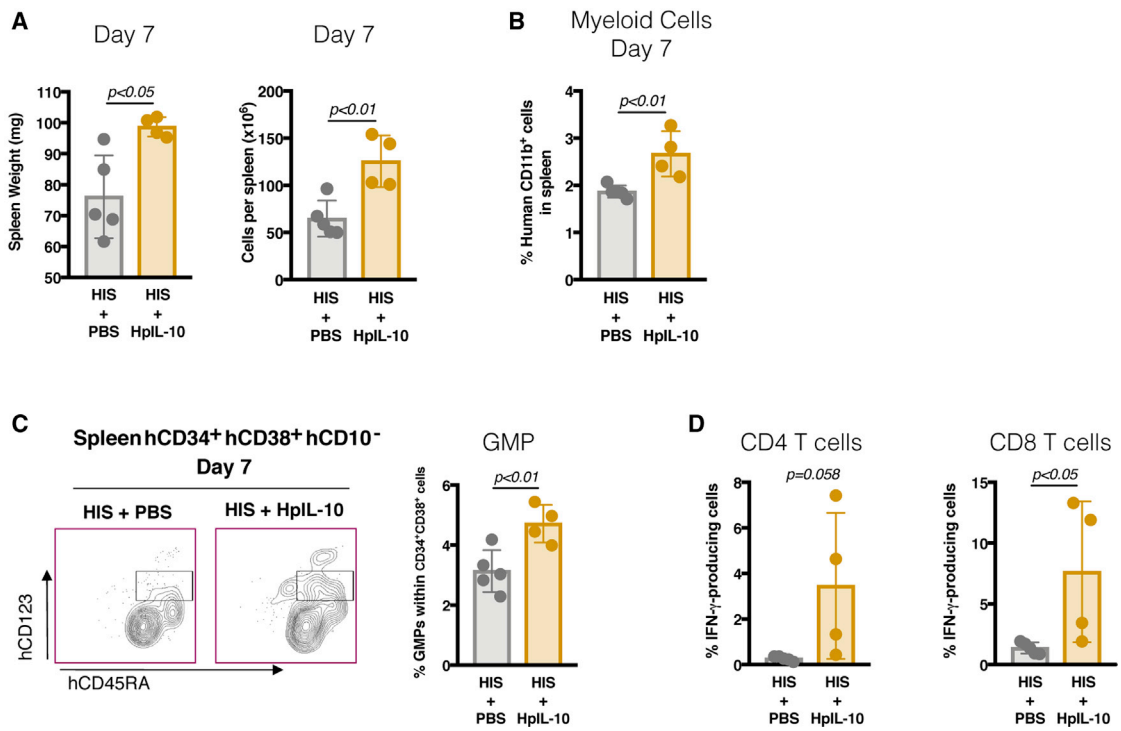

Figure 7. The IL-10-driven myelopoiesis is phenocopied in HIS mice

A human IL-10-expressing plasmid (HpIL-10) diluted in PBS was injected into NOD Prkdc^{scid} IL2Rγc$^{-/-}$ (NCG) mice reconstituted with human hematopoietic cells (HISs). Vehicle control was PBS alone.

(A) Spleen weight and total number of leukocytes determined at day 7 post injection.

(B) Percentage of human myeloid splenocytes (CD11b^{+}) was determined for PBS- and HpIL-10-injected animals.

(C) Representative plots and frequencies of splenic human GMPs (hCD45^{+} hCD34^{+} hCD10^{-} hCD123^{int} hCD45R^{+}) at day 7 after pIL-10 administration.

(D) Spleen cells from control (PBS) or induced (pIL-10) HIS mice were restimulated *ex vivo* with PMA/ionomycin in the presence of brefeldin A. The percentage of CD4 and CD8 T IFN-γ-producing cells was assessed by flow cytometry 4 h post-stimulation. Each bar represents the mean ± SD, for 4–5 mice from 1 experiment. Each dot represents a single mouse. Data were analyzed with Student's t test.

IFN-γ production by infiltrating tumor-specific CD8^{+} T cells (Emmerich et al., 2012a, 2012b; Mumm et al., 2011; Naing et al., 2016, 2018). We found that IL-10 enhanced local IFN-γ production by both αβ and γδ T cells. Moreover, induction of IL-10 led to a transcriptional and functional reprograming of both CD4 and CD8 T cells, which is compatible with that seen under strong inflammatory conditions (Kaech and Cui, 2012; Takeuchi and Saito, 2017). The IFN-γ-producing CD4 T cells are not polarized Th1 cells because they show upregulated *Eomes,* but not *Tbx21,* expression as normally observed (Cano-Gamez et al., 2020). This result is compatible with the observation that myelopoiesis (and by implication also IFN-γ expression) rapidly returns to normal once IL-10 induction is stopped. Upregulation of IFN-γ in the T cells involves indirect mechanisms because IL-10Rα$^{-/-}$ T cells are also able to mediate EM after IL-10 induction. Because EM still occurs in chimeras where only the myeloid compartment expresses the IL-10R, IFN-γ expression in T cells must be secondary to the activity of IL-10 on a myeloid population. This conclusion does not however contradict that other, direct mechanisms may also operate, as seen for CD8 T cells in a tumor model (Emmerich et al., 2012a; Mumm et al., 2011; Naing et al., 2018). Most importantly, we also show that IL-10 induces IFN-γ production by T cells, and EM, in the human hematopoietic system. Therefore, regardless of the mechanism whereby IL-10 induces IFN-γ production, our results explain the hematologic observations reported in patients receiving IL-10 therapeutically (Huhn et al., 1996, 1997, 1999). Finally, we show that the presence of either αβ and γδ T cell subsets was sufficient to promote EM in IL-10-expressing mice.

The finding that IL-10 triggers EM adds to the expanding complex network of cells and molecules affecting the hematopoietic niche (Boettcher and Manz, 2017; Gomes et al., 2020). Our findings underscore the need for further studies on the role of IL-10 in the hematopoietic alterations often seen in infection and autoimmunity. For example, both elevated levels of IL-10 (Park et al., 1998) and hematopoietic alterations, including anemia, thrombocytopenia, and lymphopenia, have been reported in Lupus patients (Budman and Steinberg, 1977). Neutropenia is frequently found, although some patients can also develop leukocytosis and neutrophilia (Velo-García et al., 2016). It is not surprising that such a complex disease as Lupus can present a diverse array of clinical manifestations, but notably, in a mouse model of Lupus, elevated serum IL-10, expansion of the LSK and GMP compartments, and myeloid-biased hematopoiesis have all been reported (Niu et al., 2013). Thus, it is tempting to speculate that IL-10 activity may have a role,

unappreciated so far, in some hematological manifestations found in Lupus. Finally, our study is directly relevant for the design of IL-10-based therapies and suggests that short-term IL-10 administration might be a useful strategy for promoting myeloid recovery after iatrogenic stress. Because IL-10 acts through a different route than the commonly used CSFs, it may provide alternative ways to overcome some described deleterious side effects and thus improve the available clinical strategies for myeloid recovery.

Limitations of the study

Although our study provides an explanation for the hematological alterations observed in humans receiving IL-10 therapeutically, some questions remain that call for further research. The mechanism by which IL-10 induces IFN-γ production by T cells *in vivo* and its relevance to disease models require further investigation; also, because the observed phenotype is initiated at the LSK level, performing single-cell RNA-seq of the LSK and LK populations may shed light on the transcriptional changes occurring in earlier progenitors; and finally, we cannot exclude that epigenomic changes induced in HSC/LSK populations by IL-10 exposure may affect their function. This issue could be addressed by performing HSC transplantation experiments.

STAR★METHODS

Detailed methods are provided in the online version of this paper and include the following:

- KEY RESOURCES TABLE
- RESOURCE AVAILABILITY
  - Lead contact
  - Materials availability
  - Data and code availability
- EXPERIMENTAL MODELS AND SUBJECT DETAILS
  - Human sample collection
  - Mice
  - *In vitro* Cell Cultures
- METHOD DETAILS
  - IL-10 induction
  - Hydrodynamic administration of the plasmids
  - BM Transplantation Assays
  - Generation of humanized mice (HIS mice)
  - Hematological parameters
  - Histology
  - Preparation of Cell Suspensions
  - Flow Cytometry and Cell Sorting
  - *Ex vivo* Restimulation
  - RNA extraction, cDNA and real time qPCR (RT-qPCR)
  - Transcriptome analyses by RNA-seq
  - Cytokine Quantification
- QUANTIFICATION AND STATISTICAL ANALYSIS

SUPPLEMENTAL INFORMATION

Supplemental information can be found online at https://doi.org/10.1016/j.celrep.2021.109887.

ACKNOWLEDGMENTS

We thank Vincent Rouilly for statistical advice and Werner Müller (University of Manchester), Rui Appelberg (i3S), and Bruno Silva-Santos (iMM) for providing the IL-10Rα-, IFN-γ-, and TCRγδ-deficient animals, respectively. We thank Anne O'Garra for helpful discussions and for critical reading of the manuscript. We also thank Delfim Duarte and Maria José Teles for helpful discussions and for helping with the hemogram quantification. We thank Caetano Reis e Sousa for help with the preparation of the graphical abstract. We thank the support of the personnel in the animal facilities, the i3S scientific platforms Translational Cytometry (TraCy), and Histology and Electron Microscopy (HEMS). HEMS is a member of the national infrastructure PPBI (Portuguese Platform of Bioimaging; PPBI-POCI-01-0145-FEDER-022122).

A. Cardoso (SFRH/BD/84704/2012) and A.C.M. (SFRH/BD/136800/2018) were supported by the Portuguese Foundation for Science and Technology (FCT) through PhD grants.

This study was partially supported by grants from the National Key Research and Development Program of China (2019YFA0802900), National Natural Science Foundation of China (32070942), and Fundamental Research Funds for the Central Universities.

The M.S. lab was financed by a FCT-ANR grant (MyeloTEN-FCTANR/ BIMEC/0007/2013). We acknowledge the GenomePT project (POCI-01-0145-FEDER-022184), supported by COMPETE 2020 - Operational Programme for Competitiveness and Internationalisation (POCI), Lisboa Portugal Regional Operational Programme (Lisboa2020), Algarve Portugal Regional Operational Programme (CRESC Algarve2020), under the PORTUGAL 2020 Partnership Agreement, through the European Regional Development Fund (ERDF), and by FCT.

This work was funded by National Funds through FCT, I.P., under the project UIDB/04293/2020, and backed by the COST Action BM1404 European Network of Investigators Triggering Exploratory Research on Myeloid Regulatory Cells (http://www.mye-euniter.eu), which is supported by the Horizon 2020—EU Framework Program Research and Innovation Programme. M.S. is funded by FCT through *Estímulo Individual ao Emprego Científico*.

A. Cumano and P.V. were financed by ANR Twothyme and by REVIVE (Investissement d'Avenir; ANR-10-LABX-73). A.B., A. Cumano, and P.V. were also financed by the Institut Pasteur, INSERM, and ANR (project MYELOTEN; ANR-13-ISV1-0003-01).

AUTHOR CONTRIBUTIONS

A. Cardoso, A.C.M., A.R.M., W.L., Y.L., A.G.C., and A.B. performed experiments. A. Cardoso, A.C.M., I.C., A.G.C., A.B., Y.L., J.P.D.S., A. Cumano, P.V., and M.S. designed experiments and analyzed data. A.R.M. conducted RNA-seq curation and analysis. A. Cardoso, P.V., and M.S. wrote the manuscript. P.V. and M.S. supervised the project. All authors reviewed and edited the manuscript.

DECLARATION OF INTERESTS

Y.L. is currently consulting for GemPharmatech Co.

Received: November 18, 2020
Revised: May 17, 2021
Accepted: October 5, 2021
Published: October 26, 2021

REFERENCES

Bach, E.A., Szabo, S.J., Dighe, A.S., Ashkenazi, A., Aguet, M., Murphy, K.M., and Schreiber, R.D. (1995). Ligand-induced autoregulation of IFN-gamma receptor beta chain expression in T helper cell subsets. Science *270*, 1215–1218.

Baldridge, M.T., King, K.Y., Boles, N.C., Weksberg, D.C., and Goodell, M.A. (2010). Quiescent haematopoietic stem cells are activated by IFN-gamma in response to chronic infection. Nature *465*, 793–797.

Becht, E., McInnes, L., Healy, J., Dutertre, C.A., Kwok, I.W.H., Ng, L.G., Ginhoux, F., and Newell, E.W. (2018). Dimensionality reduction for visualizing single-cell data using UMAP. Nat. Biotechnol *37*, 38–44.

Belyaev, N.N., Brown, D.E., Diaz, A.I., Rae, A., Jarra, W., Thompson, J., Langhorne, J., and Potocnik, A.J. (2010). Induction of an IL7-R(+)c-Kit(hi) myelolymphoid progenitor critically dependent on IFN-gamma signaling during acute malaria. Nat. Immunol. *11*, 477–485.

Belyaev, N.N., Biró, J., Langhorne, J., and Potocnik, A.J. (2013). Extramedullary myelopoiesis in malaria depends on mobilization of myeloid-restricted progenitors by IFN-γ induced chemokines. PLoS Pathog. *9*, e1003406.

Blighe, K. (2019). EnhancedVolcano: Publication-ready volcano plots with enhanced colouring and labeling. R package version 1.0.1 (Bioconductor).

Boettcher, S., and Manz, M.G. (2017). Regulation of Inflammation- and Infection-Driven Hematopoiesis. Trends Immunol. *38*, 345–357.

Boyer, S.W., Schroeder, A.V., Smith-Berdan, S., and Forsberg, E.C. (2011). All hematopoietic cells develop from hematopoietic stem cells through Flk2/Flt3-positive progenitor cells. Cell Stem Cell *9*, 64–73.

Budman, D.R., and Steinberg, A.D. (1977). Hematologic aspects of systemic lupus erythematosus. Current concepts. Ann. Intern. Med. *86*, 220–229.

Cano-Gamez, E., Soskic, B., Roumeliotis, T.I., So, E., Smyth, D.J., Baldrighi, M., Willé, D., Nakic, N., Esparza-Gordillo, J., Larminie, C.G.C., et al. (2020). Single-cell transcriptomics identifies an effectorness gradient shaping the response of CD4$^+$ T cells to cytokines. Nat. Commun. *11*, 1801.

Cardoso, A., Gil Castro, A., Martins, A.C., Carriche, G.M., Murigneux, V., Castro, I., Cumano, A., Vieira, P., and Saraiva, M. (2018). The Dynamics of Interleukin-10-Afforded Protection during Dextran Sulfate Sodium-Induced Colitis. Front. Immunol. *9*, 400.

Carlson, M. (2019). org.Mm.eg.db.Genome wide annotation for Mouse.R package version 3.8.2 (Bioconductor).

de Bruin, A.M., Libregts, S.F., Valkhof, M., Boon, L., Touw, I.P., and Nolte, M.A. (2012). IFNγ induces monopoiesis and inhibits neutrophil development during inflammation. Blood *119*, 1543–1554.

Edgar, R., Domrachev, M., and Lash, A.E. (2002). Gene Expression Omnibus: NCBI gene expression and hybridization array data repository. Nucleic Acids Res. *30*, 207–210.

Emmerich, J., Mumm, J.B., Chan, I.H., LaFace, D., Truong, H., McClanahan, T., Gorman, D.M., and Oft, M. (2012a). IL-10 directly activates and expands tumor-resident CD8(+) T cells without de novo infiltration from secondary lymphoid organs. Cancer Res. *72*, 3570–3581.

Emmerich, J., Mumm, J.B., and Oft, M. (2012b). Autochthonous T cells to the rescue: IL-10 directly activates tumor-resident CD8(+) T cells. OncoImmunology *1*, 1637–1639.

Fiorentino, D.F., Bond, M.W., and Mosmann, T.R. (1989). Two types of mouse T helper cell. IV. Th2 clones secrete a factor that inhibits cytokine production by Th1 clones. J. Exp. Med. *170*, 2081–2095.

Gomes, A.C., Saraiva, M., and Gomes, M.S. (2020). The bone marrow hematopoietic niche and its adaptation to infection. Semin. Cell Dev. Biol. *112*, 37–48.

Groux, H., Cottrez, F., Rouleau, M., Mauze, S., Antonenko, S., Hurst, S., McNeil, T., Bigler, M., Roncarolo, M.G., and Coffman, R.L. (1999). A transgenic model to analyze the immunoregulatory role of IL-10 secreted by antigen-presenting cells. J. Immunol. *162*, 1723–1729.

Huhn, R.D., Radwanski, E., O'Connell, S.M., Sturgill, M.G., Clarke, L., Cody, R.P., Affrime, M.B., and Cutler, D.L. (1996). Pharmacokinetics and immunomodulatory properties of intravenously administered recombinant human interleukin-10 in healthy volunteers. Blood *87*, 699–705.

Huhn, R.D., Radwanski, E., Gallo, J., Affrime, M.B., Sabo, R., Gonyo, G., Monge, A., and Cutler, D.L. (1997). Pharmacodynamics of subcutaneous recombinant human interleukin-10 in healthy volunteers. Clin. Pharmacol. Ther. *62*, 171–180.

Huhn, R.D., Pennline, K., Radwanski, E., Clarke, L., Sabo, R., and Cutler, D.L. (1999). Effects of single intravenous doses of recombinant human interleukin-10 on subsets of circulating leukocytes in humans. Immunopharmacology *41*, 109–117.

Istaces, N., Splittgerber, M., Lima Silva, V., Nguyen, M., Thomas, S., Le, A., Achouri, Y., Calonne, E., Defrance, M., Fuks, F., et al. (2019). EOMES interacts with RUNX3 and BRG1 to promote innate memory cell formation through epigenetic reprogramming. Nat. Commun. *10*, 3306.

Kaech, S.M., and Cui, W. (2012). Transcriptional control of effector and memory CD8+ T cell differentiation. Nat. Rev. Immunol. *12*, 749–761.

Kaufmann, E., Sanz, J., Dunn, J.L., Khan, N., Mendonça, L.E., Pacis, A., Tzelepis, F., Pernet, E., Dumaine, A., Grenier, J.C., et al. (2018). BCG Educates Hematopoietic Stem Cells to Generate Protective Innate Immunity against Tuberculosis. Cell *172*, 176–190.e19.

Khan, N., Downey, J., Sanz, J., Kaufmann, E., Blankenhaus, B., Pacis, A., Pernet, E., Ahmed, E., Cardoso, S., Nijnik, A., et al. (2020). M. tuberculosis Reprograms Hematopoietic Stem Cells to Limit Myelopoiesis and Impair Trained Immunity. Cell *183*, 752–770.e22.

Komatsu, N., and Hori, S. (2007). Full restoration of peripheral Foxp3+ regulatory T cell pool by radioresistant host cells in scurfy bone marrow chimeras. Proc. Natl. Acad. Sci. USA *104*, 8959–8964.

Korotkevich, G., Sukhov, V., Budin, N., Shpak, B., Artyomov, M.N., and Sergushichev, A. (2019). Fast gene set enrichment analysis. bioRxiv. https://doi.org/10.1101/060012.

Lang, R., Rutschman, R.L., Greaves, D.R., and Murray, P.J. (2002). Autocrine deactivation of macrophages in transgenic mice constitutively overexpressing IL-10 under control of the human CD68 promoter. J. Immunol. *168*, 3402–3411.

Li, Y., Strick-Marchand, H., Lim, A.I., Ren, J., Masse-Ranson, G., Dan Li, Jouvion, G., Rogge, L., Lucas, S., Bin Li, and Di Santo, J.P. (2017). Regulatory T cells control toxicity in a humanized model of IL-2 therapy. Nat. Commun. *8*, 1762.

Liberzon, A., Birger, C., Thorvaldsdóttir, H., Ghandi, M., Mesirov, J.P., and Tamayo, P. (2015). The Molecular Signatures Database (MSigDB) hallmark gene set collection. Cell Syst. *1*, 417–425.

McCarthy, D.J., Chen, Y., and Smyth, G.K. (2012). Differential expression analysis of multifactor RNA-Seq experiments with respect to biological variation. Nucleic Acids Res. *40*, 4288–4297.

Mercier, F.E., Sykes, D.B., and Scadden, D.T. (2016). Single Targeted Exon Mutation Creates a True Congenic Mouse for Competitive Hematopoietic Stem Cell Transplantation: The C57BL/6-CD45.1(STEM) Mouse. Stem Cell Reports *6*, 985–992.

Moore, K.W., Vieira, P., Fiorentino, D.F., Trounstine, M.L., Khan, T.A., and Mosmann, T.R. (1990). Homology of cytokine synthesis inhibitory factor (IL-10) to the Epstein-Barr virus gene BCRFI. Science *248*, 1230–1234.

Moore, K.W., de Waal Malefyt, R., Coffman, R.L., and O'Garra, A. (2001). Interleukin-10 and the interleukin-10 receptor. Annu. Rev. Immunol. *19*, 683–765.

Mumm, J.B., Emmerich, J., Zhang, X., Chan, I., Wu, L., Mauze, S., Blaisdell, S., Basham, B., Dai, J., Grein, J., et al. (2011). IL-10 elicits IFNγ-dependent tumor immune surveillance. Cancer Cell *20*, 781–796.

Naing, A., Papadopoulos, K.P., Autio, K.A., Ott, P.A., Patel, M.R., Wong, D.J., Falchook, G.S., Pant, S., Whiteside, M., Rasco, D.R., et al. (2016). Safety, Antitumor Activity, and Immune Activation of Pegylated Recombinant Human Interleukin-10 (AM0010) in Patients With Advanced Solid Tumors. J. Clin. Oncol. *34*, 3562–3569.

Naing, A., Infante, J.R., Papadopoulos, K.P., Chan, I.H., Shen, C., Ratti, N.P., Rojo, B., Autio, K.A., Wong, D.J., Patel, M.R., et al. (2018). PEGylated IL-10 (Pegilodecakin) Induces Systemic Immune Activation, CD8$^+$ T Cell Invigoration and Polyclonal T Cell Expansion in Cancer Patients. Cancer Cell *34*, 775–791.e3.

Niu, H., Fang, G., Tang, Y., Xie, L., Yang, H., Morel, L., Diamond, B., and Zou, Y.R. (2013). The function of hematopoietic stem cells is altered by both genetic and inflammatory factors in lupus mice. Blood *121*, 1986–1994.

O'Garra, A., and Vieira, P. (2007). T(H)1 cells control themselves by producing interleukin-10. Nat. Rev. Immunol. *7*, 425–428.

Oguro, H., Ding, L., and Morrison, S.J. (2013). SLAM family markers resolve functionally distinct subpopulations of hematopoietic stem cells and multipotent progenitors. Cell Stem Cell *13*, 102–116.

Ortaldo, J.R., Winkler-Pickett, R.T., Bere, E.W., Jr., Watanabe, M., Murphy, W.J., and Wiltrout, R.H. (2005). In vivo hydrodynamic delivery of cDNA encoding IL-2: rapid, sustained redistribution, activation of mouse NK cells, and therapeutic potential in the absence of NKT cells. J. Immunol. *175*, 693–699.

Ouyang, W., and O'Garra, A. (2019). IL-10 Family Cytokines IL-10 and IL-22: from Basic Science to Clinical Translation. Immunity *50*, 871–891.

Park, Y.B., Lee, S.K., Kim, D.S., Lee, J., Lee, C.H., and Song, C.H. (1998). Elevated interleukin-10 levels correlated with disease activity in systemic lupus erythematosus. Clin. Exp. Rheumatol. *16*, 283–288.

Pearce, E.L., Mullen, A.C., Martins, G.A., Krawczyk, C.M., Hutchins, A.S., Zediak, V.P., Banica, M., DiCioccio, C.B., Gross, D.A., Mao, C.A., et al. (2003). Control of effector CD8+ T cell function by the transcription factor Eomesodermin. Science *302*, 1041–1043.

Pietras, E.M., Lakshminarasimhan, R., Techner, J.M., Fong, S., Flach, J., Binnewies, M., and Passegué, E. (2014). Re-entry into quiescence protects hematopoietic stem cells from the killing effect of chronic exposure to type I interferons. J. Exp. Med. *211*, 245–262.

Pietras, E.M., Reynaud, D., Kang, Y.A., Carlin, D., Calero-Nieto, F.J., Leavitt, A.D., Stuart, J.M., Göttgens, B., and Passegué, E. (2015). Functionally Distinct Subsets of Lineage-Biased Multipotent Progenitors Control Blood Production in Normal and Regenerative Conditions. Cell Stem Cell *17*, 35–46.

Ritchie, M.E., Phipson, B., Wu, D., Hu, Y., Law, C.W., Shi, W., and Smyth, G.K. (2015). limma powers differential expression analyses for RNA-sequencing and microarray studies. Nucleic Acids Res. *43*, e47.

Robinson, M.D., McCarthy, D.J., and Smyth, G.K. (2010). edgeR: a Bioconductor package for differential expression analysis of digital gene expression data. Bioinformatics *26*, 139–140.

Rusinova, I., Forster, S., Yu, S., Kannan, A., Masse, M., Cumming, H., Chapman, R., and Hertzog, P.J. (2013). Interferome v2.0: an updated database of annotated interferon-regulated genes. Nucleic Acids Res. *41*, D1040–D1046.

Saraiva, M., Christensen, J.R., Veldhoen, M., Murphy, T.L., Murphy, K.M., and O'Garra, A. (2009). Interleukin-10 production by Th1 cells requires interleukin-12-induced STAT4 transcription factor and ERK MAP kinase activation by high antigen dose. Immunity *31*, 209–219.

Saraiva, M., Vieira, P., and O'Garra, A. (2020). Biology and therapeutic potential of interleukin-10. J. Exp. Med. *217*, e20190418.

Sato, A., Ohtsuki, M., Hata, M., Kobayashi, E., and Murakami, T. (2006). Antitumor activity of IFN-lambda in murine tumor models. J. Immunol. *176*, 7686–7694.

Schürch, C.M., Riether, C., and Ochsenbein, A.F. (2014). Cytotoxic CD8+ T cells stimulate hematopoietic progenitors by promoting cytokine release from bone marrow mesenchymal stromal cells. Cell Stem Cell *14*, 460–472.

Singhania, A., Graham, C.M., Gabryšová, L., Moreira-Teixeira, L., Stavropoulos, E., Pitt, J.M., Chakravarty, P., Warnatsch, A., Branchett, W.J., Conejero, L., et al. (2019). Transcriptional profiling unveils type I and II interferon networks in blood and tissues across diseases. Nat. Commun. *10*, 2887.

Smith, J.N.P., Zhang, Y., Li, J.J., McCabe, A., Jo, H.J., Maloney, J., and MacNamara, K.C. (2018). Type I IFNs drive hematopoietic stem and progenitor cell collapse via impaired proliferation and increased RIPK1-dependent cell death during shock-like ehrlichial infection. PLoS Pathog. *14*, e1007234.

Sosman, J.A., Verma, A., Moss, S., Sorokin, P., Blend, M., Bradlow, B., Chachlani, N., Cutler, D., Sabo, R., Nelson, M., et al. (2000). Interleukin 10-induced thrombocytopenia in normal healthy adult volunteers: evidence for decreased platelet production. Br. J. Haematol. *111*, 104–111.

Subramanian, A., Tamayo, P., Mootha, V.K., Mukherjee, S., Ebert, B.L., Gillette, M.A., Paulovich, A., Pomeroy, S.L., Golub, T.R., Lander, E.S., and Mesirov, J.P. (2005). Gene set enrichment analysis: a knowledge-based approach for interpreting genome-wide expression profiles. Proc. Natl. Acad. Sci. USA *102*, 15545–15550.

Sudo, T., Yokota, T., Oritani, K., Satoh, Y., Sugiyama, T., Ishida, T., Shibayama, H., Ezoe, S., Fujita, N., Tanaka, H., et al. (2012). The endothelial antigen ESAM monitors hematopoietic stem cell status between quiescence and self-renewal. J. Immunol. *189*, 200–210.

Szabo, S.J., Kim, S.T., Costa, G.L., Zhang, X., Fathman, C.G., and Glimcher, L.H. (2000). A novel transcription factor, T-bet, directs Th1 lineage commitment. Cell *100*, 655–669.

Takeuchi, A., and Saito, T. (2017). CD4 CTL, a Cytotoxic Subset of $CD4^+$ T Cells, Their Differentiation and Function. Front. Immunol. *8*, 194.

Tilg, H., Ulmer, H., Kaser, A., and Weiss, G. (2002a). Role of IL-10 for induction of anemia during inflammation. J. Immunol. *169*, 2204–2209.

Tilg, H., van Montfrans, C., van den Ende, A., Kaser, A., van Deventer, S.J., Schreiber, S., Gregor, M., Ludwiczek, O., Rutgeerts, P., Gasche, C., et al. (2002b). Treatment of Crohn's disease with recombinant human interleukin 10 induces the proinflammatory cytokine interferon gamma. Gut *50*, 191–195.

Velo-García, A., Castro, S.G., and Isenberg, D.A. (2016). The diagnosis and management of the haematologic manifestations of lupus. J. Autoimmun. *74*, 139–160.

Vieira, P., de Waal-Malefyt, R., Dang, M.N., Johnson, K.E., Kastelein, R., Fiorentino, D.F., deVries, J.E., Roncarolo, M.G., Mosmann, T.R., and Moore, K.W. (1991). Isolation and expression of human cytokine synthesis inhibitory factor cDNA clones: homology to Epstein-Barr virus open reading frame BCRFI. Proc. Natl. Acad. Sci. USA *88*, 1172–1176.

Warnes, G.R., Bolker, B., Lumley, T., Warnes, G.R., Bonebakker, L., Gentleman, R., Liaw, W.H.A., Maechler, M., Magnusson, A., Moeller, S., et al. (2020). gplots: Various R Programming Tools for Plotting Data. R package version 3.0.1.2 (ScienceOpen.com).

Yang, Y., Xu, J., Niu, Y., Bromberg, J.S., and Ding, Y. (2008). T-bet and eomesodermin play critical roles in directing T cell differentiation to Th1 versus Th17. J. Immunol. *181*, 8700–8710.

STAR★METHODS

KEY RESOURCES TABLE

REAGENT or RESOURCE	SOURCE	IDENTIFIER
Antibodies		
PE anti-mouse/human B220 (clone RA3-6B2)	Biolegend	Cat# 103208; RRID:AB_312993
Biotin anti-mouse/human B220 (clone RA3-6B2)	Biolegend	Cat# 103204; RRID:AB_312989
Biotin anti-mouse/human B220 (clone RA3-6B2)	Sony	1116020
APC anti-mouse CCR7 (clone 4B12)	Biolegend	Cat# 120108; RRID:AB_389234
FITC anti-human CD10 (clone HI10a)	Biolegend	Cat# 312208; RRID:AB_314919
APC/Cyanine7 anti-mouse CD117 (clone 2B8)	Biolegend	Cat# 105826; RRID:AB_1626278
human CD11b (clone ICFR44)	BD	Cat# 562399; RRID:AB_2737613
Biotin anti-mouse/human CD11b (clone M1/70)	Biolegend	Cat# 101204; RRID:AB_312787
FITC anti-mouse/human CD11b (clone M1/70)	Biolegend	Cat# 101206; RRID:AB_312789
PerCP/Cyanine5.5 anti-mouse/human CD11b (clone M1/70)	Biolegend	Cat# 101228; RRID:AB_893232
APC/Cyanine7 anti-mouse/human CD11b (clone M1/70)	Biolegend	Cat# 101226; RRID:AB_830642
PE/Cyanine7 anti-mouse CD11c (clone N418)	Biolegend	Cat# 117318; RRID:AB_493568
Biotin anti-mouse CD11c (clone N418)	Biolegend	Cat# 117304; RRID:AB_313773
Biotin anti-mouse CD11c (clone N418)	Sony	1186515
APC anti-human CD123 (clone 6H6)	Biolegend	Cat# 306012; RRID:AB_439779
PE/Cyanine7 anti-mouse CD127 (IL7Rα; clone A7R34)	Biolegend	Cat# 135014; RRID:AB_1937265
Biotin anti-mouse CD127 (IL7Rα; clone A7R34)	Biolegend	Cat# 135006; RRID:AB_2126118
PE anti-mouse CD135 (Flt3; clone A2F10)	Biolegend	Cat# 135306; RRID:AB_1877217
FITC anti-human CD14 (clone HCD14)	Biolegend	Cat# 325604; RRID:AB_830677
Brilliant Violet 711 anti-mouse CD150 (cloneTC15-12F12.2)	Biolegend	Cat# 115941; RRID:AB_2629660
Purified CD16/32 (FcBlock; (clone 24G2)	BD	553141
PE anti-mouse CD16/32 (FcγR; (clone 93)	Biolegend	Cat# 101308; RRID:AB_312807
PerCP/Cyanine5.5 anti-mouse CD16/32 (FcγR; (clone 93)	Biolegend	Cat# 101324; RRID:AB_1877267
APC/Cyanine7 anti-mouse CD19 (clone 6D5)	Biolegend	Cat# 115530; RRID:AB_830707
Biotin anti-mouse CD19 (clone 6D5)	Biolegend	Cat# 115504; RRID:AB_313639
FITC anti-mouse CD19 (clone 6D5)	Biolegend	Cat# 115506; RRID:AB_313641
PE/Cyanine7 anti-mouse CD19 (clone 6D5)	Biolegend	Cat# 115520; RRID:AB_313655
PE anti-human CD19 (clone HIB19)	Biolegend	Cat# 302208; RRID:AB_314238
APC/Cyanine7 anti-human CD3 (clone UCHT1)	Biolegend	Cat# 300426; RRID:AB_830755
PerCP/Cyanine5.5 anti-human CD3 (clone UCHT1)	Biolegend	Cat# 300430; RRID:AB_893299
Brilliant Violet 421 anti-human CD34 (clone 581)	BD	Cat# 562577, RRID:AB_2687922
Alexa Fluor 647 anti-mouse CD34 (clone RAM34)	BD	Cat# 560233; RRID:AB_1645199
eFluor 450 anti-mouse CD34 (clone RAM34)	Invitrogen	Cat# 48-0341-82; RRID:AB_2043837
Brilliant Violet 650 anti-mouse CD38 (clone 90/CD38)	BD	740361
FITC anti-human CD38 (clone HIT2)	Biolegend	Cat# 303504; RRID:AB_314356
Biotin anti-mouse CD3ε (clone 145-2C11)	Biolegend	Cat# 100304; RRID:AB_312669
PerCP/Cyanine5.5 anti-mouse CD3ε (clone 145-2C11)	Biolegend	Cat# 100328; RRID:AB_893318
Brilliant Violet 785 anti-mouse CD3ε (clone 145-2C11)	Biolegend	Cat# 100355; RRID:AB_2565969
Pacific Blue anti-human CD3ε (clone 500A2)	BD	Cat# 558214; RRID:AB_397063
Brilliant Violet 650 anti-human CD4 (clone SK3)	BD	563875
APC/Cyanine7 anti-human CD4 (clone A161A1)	Biolegend	Cat# 357416; RRID:AB_2616810

(*Continued on next page*)

Continued

REAGENT or RESOURCE	SOURCE	IDENTIFIER
APC/Cyanine7 anti-mouse CD4 (clone GJ1.5)	Biolegend	Cat# 100414; RRID:AB_312699
Biotin anti-mouse CD4 (clone GJ1.5)	Biolegend	Cat# 100404; RRID:AB_312689
Brilliant Violet 785 anti-mouse CD4 (clone GJ1.5)	Biolegend	Cat# 100453; RRID:AB_2565843
PE/Cyanine5 anti-mouse CD44 (clone IM7)	Biolegend	Cat# 103010; RRID:AB_312961
PE/Cyanine7 anti-human CD45 (clone 2D1)	Biolegend	Cat# 368532; RRID:AB_2715892
APC/Cyanine7 anti-mouse CD45 (clone 30-F11)	Biolegend	Cat# 103116; RRID:AB_312981
Brilliant Violet 711 anti-mouse CD45 (clone 30F11)	Biolegend	Cat# 103147; RRID:AB_2564383
Brilliant Violet 605 anti-human CD45 (clone HI30)	Biolegend	Cat# 304042; RRID:AB_2562106
Brilliant Violet 711 anti-human CD45 (clone HI30)	Biolegend	Cat# 304050; RRID:AB_2563466
Brilliant Violet 510 anti-mouse CD45.1 (clone A20)	Biolegend	Cat# 110741; RRID:AB_2563378
FITC anti-mouse CD45.1 (clone A20)	Biolegend	Cat# 110706; RRID:AB_313495
PE anti-mouse CD45.1 (clone A20)	Biolegend	Cat# 110708; RRID:AB_313497
PE/Cyanine7 anti-mouse CD45.1 (clone A20)	Biolegend	Cat# 110730; RRID:AB_1134168
Brilliant Violet 650 anti-mouse CD45.2 (clone 104)	Biolegend	Cat# 109836; RRID:AB_2563065
Brilliant Violet 785 anti-mouse CD45.2 (clone 104)	Biolegend	Cat# 109839; RRID:AB_2562604
PE/Cyanine7 anti-mouse CD45.2 (clone 104)	Biolegend	Cat# 109830; RRID:AB_1186098
Brilliant Violet 711 anti-human CD45RA (clone HI100)	Biolegend	Cat# 304138; RRID:AB_2563815
APC/Fire 750 anti-mouse CD48 (clone HM48-1)	Biolegend	Cat# 103446; RRID:AB_2650847
APC anti-mouse CD48 (clone HM48-1)	Biolegend	Cat# 103412; RRID:AB_571997
APC anti-mouse CD48 (clone HM48-1)	Sony	1117055
PE/Cyanine7 anti-mouse CD62L (MEL-14)	Biolegend	Cat# 104418; RRID:AB_313103
PE anti-mouse CD64 (clone X54-5/7.1)	Biolegend	Cat# 139304; RRID:AB_10612740
PE-CF594 anti-human CD8 (clone RPA-T8)	BD	562282
Biotin anti-mouse CD8α (clone 53-6.7)	Biolegend	Cat# 100704; RRID:AB_312743
FITC anti-mouse CD8α (clone 53-6.7)	Biolegend	Cat# 100706; RRID:AB_312745
Brilliant Violet 421 anti-mouse CD8α (clone 53-6.7)	Biolegend	Cat# 100753; RRID:AB_2562558
Brilliant Violet 650 anti-mouse CD8α (clone 53-6.7)	Biolegend	Cat# 100742; RRID:AB_2563056
PE/Cyanine7 anti-mouse CD8α (clone 53-6.7)	Biolegend	Cat# 100722; RRID:AB_312761
Biotin anti-mouse CD8α (clone 53-6.7)	Sony	1103515
Brilliant Violet 605 anti-mouse CXCR3 (clone CXCR3-173)	Biolegend	Cat# 126523; RRID:AB_2561353
APC anti-mouse ESAM (clone 1G8/ESAM)	Biolegend	Cat# 136207; RRID:AB_2101658
Biotin anti-mouse Gr1 (clone RB6-8C5)	Biolegend	Cat# 108404; RRID:AB_313369
APC anti-mouse Gr1 (clone RB6-8C5)	Biolegend	Cat# 108412; RRID:AB_313377
FITC anti-mouse Gr1 (clone RB6-8C5)	Biolegend	Cat# 108406, RRID:AB_313371
PerCP/Cyanine5.5 anti-mouse Gr1 (clone RB6-8C5)	Biolegend	Cat# 108428; RRID:AB_893558
Biotin anti-mouse Gr1 (clone RB6-8C5)	Sony	1142015
PE anti-mouse IFN-γ (clone XMG1.2)	Biolegend	Cat# 505808; RRID:AB_315402
FITC anti-mouse IFN-γ (clone XMG1.2)	Biolegend	Cat# 505806; RRID:AB_315400
PerCP/Cyanine5.5 anti-human IFNγ (clone 4S.B3)	Biolegend	Cat# 502526; RRID:AB_961355
Brilliant Violet 711 anti-mouse KLRG-1(clone 2F1)	BD	564014
Pacific Blue anti-mouse Ly6C (clone HK1.4)	Biolegend	Cat# 128014; RRID:AB_1732079
PerCP/Cyanine5.5 anti-mouse Ly6G (clone 1A8)	Biolegend	Cat# 127616; RRID:AB_1877271
Biotin anti-mouse NK1.1 (clone PK136)	Biolegend	Cat# 108704; RRID:AB_313391
Brilliant Violet 421 anti-mouse NK1.1 (clone PK136)	Biolegend	Cat# 108741, RRID:AB_2562561
Brilliant Violet 785 anti-mouse NK1.1 (clone PK136)	Biolegend	Cat# 108749; RRID:AB_2564304
Biotin anti-mouse NK1.1 (clone PK136)	Sony	1143515
Pacific Blue anti-mouse PD1 (clone EH12.2H7)	Biolegend	Cat# 329916; RRID:AB_2283437
FITC anti-mouse Sca1 (clone D7)	Biolegend	Cat# 108106; RRID:AB_313343

(*Continued on next page*)

Continued

REAGENT or RESOURCE	SOURCE	IDENTIFIER
Brilliant Violet 605 anti-mouse Sca1 (clone D7)	Biolegend	Cat# 108133, RRID:AB_2562275
FITC anti-mouse Sca1 (clone E13-161.7)	Biolegend	Cat# 122505; RRID:AB_756190
APC anti-mouse Siglec-F (clone S170007L)	Biolegend	Cat# 155508; RRID:AB_2750237
PE/Cyanine7 Streptavidin	Biolegend	405206
Brilliant Violet 785 Streptavidin	Biolegend	405249
Pacific Blue Streptavidin	Invitrogen	S11222
APC anti-mouse TCRδ (clone GL3)	Biolegend	Cat# 118116; RRID:AB_1731813
PE anti-mouse TCRδ (clone GL3)	Biolegend	Cat# 118108; RRID:AB_313832
Biotin anti-mouse Ter119 (clone TER-119)	Biolegend	Cat# 116204; RRID:AB_313705
Biotin anti-mouse Ter119 (clone TER-119)	Sony	1181015
Fixable viability dye eFlour506	Invitrogen	65-0866-18
Propidium Iodide	Sigma-Aldrich	P4864
Zombie Aqua Fixable Viability Kit	Biolegend	423102
Zombie Green Fixable Viability Kit	Biolegend	423112
Chemicals, peptides, and recombinant proteins		
Anti-biotin microbeads	Miltenyi Biotec	130-090-485
Brefeldin A	Sigma-Aldrich	B7651
Collagenase D	Sigma-Aldrich	11088858001
Erythropoietin (Epo)	R&D Systems	959-ME
Ficoll-Hypaque	Cytiva	80648356
Golgi-plug (Brefeldin A)	BioGems	2031560
Granulocyte-macrophage colony-stimulating factor (GM-CSF)	Cell line supernatant	N/A
Ionomycin calcium salt	Sigma-Aldrich	I0634
Ionomycin calcium salt	BioGems	5608212
Kit ligand (Kit-L)	Cell line supernatant	N/A
Macrophage colony-stimulating factor (M-CSF)	Supernatant of myeloma cell line	F. Melchers
Paraformaldehyde	Sigma-Aldrich	P6148
Penicillin-Streptomycin	GIBCO	15070-063
Phorbol myristate acetate (PMA)	Sigma-Aldrich	P1585
Phorbol myristate acetate (PMA)	BioGems	1652981
Sucrose	Sigma-Aldrich	S5016
Thrombopoietin (Tpo)	R&D Systems	488-TPO
Zinc sulfate heptahydrate	Sigma-Aldrich	Z4750
β-mercaptoethanol	GIBCO	31350-010
Critical commercial assays		
Direct CD34 Progenitor Cell Isolation Kit	Miltenyi Biotec	130-046-703
Foxp3/ Transcription Factor Staining Buffer Set	Invitrogen	72-5775-40
IL-10 ELISA Kit	R&D Systems	M1000B
Ion AmpliSeq Transcriptome Mouse Gene Expression Kit	ThermoFisher Scientific	A36553
Ion Xpress Barcode Adapters	ThermoFisher Scientific	4471250
Ion 550™ Kit-Chef	ThermoFisher Scientific	A34541
Ion 550™ Chip Kit	ThermoFisher Scientific	A34537
Maxi-prep Kit	Promega	A2392
Maxima SYBR Green/ROX qPCR Master Mix	ThermoFisher Scientific	K0221
Plasmid-Maxi kit	Vazyme Biotech	DC202-1

(*Continued on next page*)

Continued

REAGENT or RESOURCE	SOURCE	IDENTIFIER
PrimeScript RT Reagent kit	Takara	RR037A
Procarta Plex	Invitrogen	*Customized Panel*
ProtoScript First Strand cDNA Synthesis kit	New England Biolabs	E6300S
RNeasy Micro kit	QIAGEN	74004
TaqMan Universal Master Mix	Applied Biosystems	4304437
TaqMan Gene Expression Master Mix	Applied Biosystems	4369016
Deposited data		
BM progenitors targeted RNA-seq	NCBI Gene Expression Omnibus	GSE147195
T cell targeted RNA-seq	NCBI Gene Expression Omnibus	GSE172060
Experimental models: Organisms/strains		
C57BL/6-Ly5.1 mice	Charles River	N/A
C57BL/6J mice	Envigo/ i3S	N/A
CD3$\varepsilon^{-/-}$ mice	Institut Pasteur, Paris	N/A
IFN$\gamma^{-/-}$ mice	Rui Appleberg (i3S, Porto)	N/A
IL-10R$\alpha^{-/-}$ mice	Werner Muller (University of Manchester)	N/A
NOD Prkdc^{scid} IL2Rγc$^{-/-}$	GemPharmatech	T001475
pMT-10 mice	Paulo Vieira and Margarida Saraiva (Institute Pasteur, Paris and i3S, Porto)	N/A
Rag.γc$^{-/-}$ mice	Institut Pasteur, Paris	N/A
TCR$\delta^{-/-}$ mice	Bruno Silva-Santos (IMM, Lisbon)	N/A
μMT$^{-/-}$ mice	Institut Pasteur, Paris	N/A
Biological samples		
Human fetal liver CD34^{+}CD38^{-} cells	Drum Tower Hospital	N/A
Oligonucleotides		
Oligonucleotides	See Table S1	See Table S1
Hprt probe	Applied Biosystems	Mm03024075
Hprt probe	Applied Biosystems	Mm01545399
cEbpα probe	Applied Biosystems	Mm00514283
EpoR probe	Applied Biosystems	Mm00833882
Il-10Rα probe	Applied Biosystems	Mm00434147
Il-10Rα probe	Applied Biosystems	Mm00434151
Il-10Rβ probe	Applied Biosystems	Mm00434157
Ifnγr1 probe	Applied Biosystems	Mm00599890
Ifnγr2 probe	Applied Biosystems	Mm00492626
Recombinant DNA		
Empty Plasmid	Origene	PS100001
Human IL-10 expression plasmid	Origene	SC300099
Mouse IL-10 expression plasmid	Origene	MC208764
Software and algorithms		
CFX Manager	Bio-rad	https://www.bio-rad.com/en-uk/sku/1845000-cfx-manager-software?ID=1845000
Dimensionality reduction for visualizing single-cell data using UMAP (R package)	Becht et al., 2018	https://codeload.github.com/lmcinnes/umap/tar.gz/0.2.4

(*Continued on next page*)

Continued

REAGENT or RESOURCE	SOURCE	IDENTIFIER
Edge R (R package)	Ritchie et al., 2015	https://bioconductor.org/packages/release/bioc/html/edgeR.html
EnhancedVolcano	Blighe, 2019	https://github.com/kevinblighe/EnhancedVolcano
Fgsea (R package)	Korotkevich et al., 2019	https://github.com/ctlab/fgsea
FlowJo	FlowJo LLC	https://www.flowjo.com
Gplots (R package)	Warnes et al., 2020	https://cran.r-project.org/web/packages/gplots/index.html
GraphPad Prism v6 and v8.1.0	GraphPad Software	https://www.graphpad.com
Limma (R package)	Ritchie et al., 2015	https://bioconductor.org/packages/release/bioc/html/limma.html
org.Mm.eg.db (R package)	Carlson, 2019	https://bioconductor.org/packages/release/data/annotation/html/org.Mm.eg.db.html
R Studio v1.2.5	R Studio	https://www.rstudio.com
R v4.03	R project	https://www.r-project.org

RESOURCE AVAILABILITY

Lead contact

Further information and requests for resources and reagents should be directed to and will be fulfilled by the lead contact, Margarida Saraiva (margarida.saraiva@ibmc.up.pt).

Materials availability

This study did not generate new unique reagents.

Data and code availability

- The BM progenitors and BM T cells RNA-seq data reported in this paper have been deposited at NCBI's Gene Expression Omnibus (Edgar et al., 2002) and are publicly available as of the date of publication. Accession numbers are listed in the key resources table. All original data reported in this paper will be shared by the lead contact upon request.
- This paper does not report original code.
- Any additional information required to reanalyze the data reported in this paper is available from the lead contact upon request.

EXPERIMENTAL MODELS AND SUBJECT DETAILS

Human sample collection

Human CD34^{+} cells were collected from 14- to 20- week-old fetal liver tissues under clinical ethical approval from ethical committee of Drum Tower Hospital with informed consent (protocol # 2021-488-01).

Mice

C57BL/6 mice were purchased from Janvier Labs or Charles River, pMT-10 mice, IL-10R$\alpha^{-/-}$ mice, pMT-10.IL-10R$\alpha^{-/-}$ mice (pMT-10^{Tg+} IL-10R$\alpha^{-/-}$), μMT$^{-/-}$ mice, Rag.γc$^{-/-}$ mice (Rag2$^{-/-}$ γc$^{-/-\ or\ y/-}$), CD3$\varepsilon^{-/-}$ mice, TCR$\delta^{-/-}$ mice, IFNγ $^{-/-}$ mice, pMT-10.Rag.γc$^{-/-}$ mice (pMT-10^{Tg+} Rag2$^{-/-}$ γc$^{-/-\ or\ y/-}$), pMT-10.CD3$^{-/-}$ mice (pMT-10^{Tg+} CD3$\varepsilon^{-/-}$), pMT-10.IFNγ $^{-/-}$ mice (pMT-10^{Tg+} IFNγ $^{-/-}$), pMT-10.TCR$\delta^{-/-}$ mice (pMT-10^{Tg+} TCR$\delta^{-/-}$), and pMT-10.M$\mu^{-/-}$ mice (pMT-10^{Tg+} M$\mu^{-/-}$) were bred either at the ICVS, i3S or the Pasteur Institute under specific pathogen-free conditions. Animal experiments were done in strict accordance with recommendations of the European Union Directive 2010/63/EU and previously approved by Portuguese National Authority for Animal Health–Direção Geral de Alimentação e Veterinária (DGAV; (#014811/2016-07-13), by the i3S Animal Ethics Committee and by the Pasteur Institute Safety Committee. Mice were maintained with food and water *ad libitum* and euthanized by CO_2 inhalation or cervical dislocation with efforts to minimize suffering. NOD Prkdc^{scid} IL2Rγc$^{-/-}$ (NCG) mice were obtained from Gempharmatech (T001475). NCG mice were housed in individual ventilated cages under specific pathogen-free conditions with humane care in National Resource Center for Mutant Mice (NRCMM). All experiments involving the generation and characterization of humanized mice

were approved by an Institutional Animal Care and Use Committee (IACUC) at the Model Animal Research Center in Nanjing University (AP# LY-01). Mice were used at 5-12 weeks of age and sex-matched for experiments.

In vitro Cell Cultures

Single cells from CMP, GMPs and MEPs subsets were sorted into 60-well Terasaki plates containing 30 μL of differentiation medium (optiMEM (GIBCO; 51985-026) containing 20% FCS, Penicillin (50 units/mL), Streptomycin (50 μg/mL) and β-mercaptoethanol (50 μM), and supplemented with a saturating concentration of the following cytokines: macrophage colony-stimulating factor (M-CSF; > 10 ng/ml), granulocyte-macrophage colony-stimulating factor (GM-CSF; > 10 ng/ml), c-Kit ligand (Kitl; > 10 ng/ml), Erythropoietin (Epo; > 4U/ml) and Thrombopoietin (Tpo; > 100 ng/ml). Cultures were supplemented with fresh cytokines at day 3. Frequency scores were assigned based on the frequency of colony-positive wells at day 4 of culture. At day 7 of culture, cells were transferred to a slide using a Cytopsin centrifuge at 600 rpm for 4 min at room temperature. Slides were stained with May-Grünwald for 5 min, washed with PBS and stained with Giemsa for 15 min. Slides were rinsed with deionized water, and dried.

METHOD DETAILS

IL-10 induction

IL-10 overexpression was induced via administration of Zn sulfate heptahydrate ($ZnSO_4.7H_2O$) in the drinking water as reported (Cardoso et al., 2018). A solution of 50 nM Zn with 2% sucrose was fed to the mice *ad libitum*, during the experimental period.

Hydrodynamic administration of the plasmids

Mouse and human IL-10 expression plasmids and control empty plasmids were purified by either Maxi-prep Kit or Plasmid-Maxi kit with endotoxin removal. Hydrodynamic injection was performed as reported (Li et al., 2017). Briefly, we used 27-gauge needles to inject a blood volume equivalent of PBS containing mouse (30 μg) or human (50 μg) IL-10 plasmids into BL/6 and pMT-10.IL-10R$\alpha^{-/-}$ or HIS mice within 7 s.

BM Transplantation Assays

Lethally irradiated (850 rad) 1) pMT-10.CD3$^{-/-}$ 5.2 were grafted with 4x10^6 of CD3, TCRβ and TCRγδ-depleted BM cells isolated from BL/6 5.1 mice or TCR$\alpha^{-/-}$ 5.2 mice; 2) pMT-10.IL-10R$\alpha^{-/-}$ mice 5.2 were grafted with 4x10^6 of CD3, TCRβ and TCRγδ-depleted BM cells isolated from BL/6 5.1, IL-10R$\alpha^{-/-}$ 5.2 mice or non-depleted BM cells isolated from pMT-10.Rag.γc$^{-/-}$ mice; 3) pMT-10.IL-10R$\alpha^{-/-}$ mice 5.2 were grafted with 4x10^6 of CD3, TCRβ and TCRγδ-depleted BM cells isolated from BL/6 5.1 or a mix (1:1) of BL/6 5.1 and IL-10R$\alpha^{-/-}$ mice. Magnetic separation was used for CD3, TCRβ and TCRγδ-depletion (LS columns; Miltenyi Biotec 130-042-401). Donor reconstitution was assessed by peripheral blood analysis 4 weeks after transplantation.

Generation of humanized mice (HIS mice)

Human fetal liver tissue was cut into small pieces of 1∼2 mm and digested with preheated DMEM supplemented with 5mg/100ml DNase I, 50mg/100ml Collagenase D, 1% Penicillin/Streptomycin and 2% FCS at 37°C for 30 minutes. The cell suspension was filtered through a 70 μm cell strainer and centrifuged at 500 g for 10 min. Mononuclear cells were obtained from resuspended pellet by Ficoll-Hypaque density gradient centrifugation. CD34$^+$ cells were purified by Direct CD34 Progenitor Cell Isolation Kit and subsequently phenotyped for CD38 expression. Newborn pups (4-6 days old) received sublethal irradiation (70cGy), and then intrahepatic injection of 5x10^4 CD34$^+$CD38$^-$ human fetal liver cells. After 10 weeks of humanization, 50 μL blood was drawn from each mouse to check human cell reconstitution. Mice with more than 1x10^5/ml human CD45$^+$ cells in the blood were used for subsequent experiments.

Hematological parameters

Blood was collected by retro-orbital or cardiac puncture under anesthesia (terminal bleeding). One hundred and fifty to two hundred and fifty microliters of blood was collected to EDTA tubes (BD Vacutainer). Blood parameters were blindly analyzed in certified laboratories (CoreLab, Centro Hospitalar do Porto, Porto, Portugal and SegaLab, Porto, Portugal). The analysis was performed using a Sysmex XE-5000 hematology analyzer or a Siemens Advia 120.

Histology

Spleen samples were fixed in 4% paraformaldehyde (PFA) immediately after mice were sacrificed. The 3 μm paraffin-embedded sections were stained with hematoxylin and eosin. Images were acquired on a NanoZoomer 2.0HT (Hamamatsu).

Preparation of Cell Suspensions

Lymphoid organs – femurs, tibias, thymus and spleens – were recovered into Hank's Balanced Solution (HBSS; GIBCO 24020-091) or Phosphate Buffered Saline (PBS; GIBCO 14190144) with 2%–4% of Fetal Calf Serum (FCS; Eurobio CVFSVF000U). BM cells were extracted by flushing the femurs and tibias with 2mL of HBBS or PBS supplemented with 2%–4% of FCS. Thymus and spleens were mechanically disaggregated with curved tweezers to obtain single cell suspensions. Cell suspensions were filtered with a 70 μm

nylon mesh and cell numbers were estimated using CountBright Absolute Counting beads (Invitrogen) or Cellometer Auto T4 Bright (Nexcelom).

Flow Cytometry and Cell Sorting

Cell suspensions were stained with antibodies listed in the Key Resources Table. Stained cells were analyzed on LSR Fortessa, LSR II or Canto II or purified through a FACSAria II or III (all from BD Biosciences). Data were analyzed on FlowJo software v10.5.3. Flow Cytometry Standard (FCS) files were exported from FlowJo for analysis by Uniform Manifold Approximation and Projection (UMAP) performed in R (Becht et al., 2018).

Ex vivo Restimulation

Mouse BM cells were washed, plated at $1x10^6$ cells/well in complete medium (RMPI 1640, GIBCO 31870025; 10% FCS; 1% HEPES, GIBCO H0887-100ml) and restimulated *in vitro* with phorbol myristate acetate (PMA; 50 ng/ml) and ionomycin calcium salt (500 ng/ml) in the presence of brefeldin A (10 ng/ml) for 4h at 37°C.

Spleen cells from HIS mice were stimulated with 50 ng/ml PMA and 1 μg/ml ionomycin for 4h in the presence of Golgi-plug. After restimulation, IFN-γ production by T cells was accessed by flow cytometry as described above.

RNA extraction, cDNA and real time qPCR (RT-qPCR)

Sorted samples were isolated directly into lysis buffer of RNeasy Micro Kit and kept at −80°C until RNA extraction. mRNA, from CMPs, GMPs, MEPs and mature T cell subsets, was extracted using RNeasy Micro kit and converted into cDNA by reverse transcription with PrimeScript RT Reagent kit or ProtoScript First Strand cDNA Synthesis kit. Expression levels were determined by RT-qPCR using Taqman primers (*Hprt, cEbpα, EpoR*, *Il-10Rα, Il-10Rβ, Ifnγr1* and *Ifnγr2*) and Taqman Universal Master Mix. *Ifng*, *Eomes*, *Tbet* and *Ubiqutin* expression were determined using Maxima SYBR Green/ROX qPCR Master Mix and specific oligonucleotides (sequences in Table S2). qRT-PCR reactions were performed on an ABI 7300 thermocycler (Applied Biosystems), CFX96 or CFX 384 PCR System (Biorad). Gene relative expression was determined using the 2ΔCt method.

Transcriptome analyses by RNA-seq

Targeted RNA sequencing was performed by GenCore, i3S (Instituto de Investigação e Inovação em Saúde) using Ion AmpliSeq Transcriptome Mouse Gene Expression Kit. All subsequent analyses were performed in R. RNA expression levels in the count matrix were normalized using the trimmed mean of M-values and computed as counts per million using edgeR (McCarthy et al., 2012; Robinson et al., 2010) . Differential expression analysis was performed using both edgeR and limma (Ritchie et al., 2015) on genes with more than 15 raw counts in all samples. Differentially expressed genes were determined through linear model fitting and Empirical Bayes moderated t-statistics test. Genes with adjusted p value ≤ 0.05 and log2 fold-change ≤ -2 or ≥ 2 were considered differentially and significantly expressed. Gene set enrichment analysis (GSEA) was performed using FGSEA package (Korotkevich et al., 2019) and MSigDB hallmark gene sets (Liberzon et al., 2015; Subramanian et al., 2005) for mouse. IFN-γ related genes were identified using Interferome database or a recently identified IFN-γ-related module (Rusinova et al., 2013; Singhania et al., 2019). A Z-score for each gene was calculated and presented on the heatmaps. Volcano plots and heatmaps were obtained with EnhancedVolcano (Blighe, 2019) and gplots (Warnes et al., 2020), respectively.

Cytokine Quantification

IL-10 concentration in the serum was quantified using a commercially available ELISA kit or using a costume made ProcartaPlex immunoassay. IL-6, G-CSF, M-CSF, GM-CSF, IL-1β, TNF-α, IFN-α and IFN-γ were measured using a costume made ProcartaPlex immunoassay.

QUANTIFICATION AND STATISTICAL ANALYSIS

Statistical significance was determined using Student's t test, one-way analysis of variance (ANOVA) or two-way ANOVA as indicated in the figure legends. Outliers were identified using ROUT. Graphs containing errors bars show means ± SD. Statistically significant values are indicated in the figures. These tests were performed with Prism Software (GraphPad).